Title
Substrate-induced changes in the structural properties of LacY

Journal
Proceedings of the National Academy of Sciences of the United States of America, 111(16)

ISSN
0027-8424

Authors
Serdiuk, Tetiana
Madej, M Gregor
Sugihara, Junichi
et al.

Publication Date
2014-04-22

DOI
10.1073/pnas.1404446111

Peer reviewed

Substrate-induced changes in the structural properties of LacY

Tetiana Serdiuk[a], M. Gregor Madej[b], Junichi Sugihara[b], Shiho Kawamura[a], Stefania A. Mari[a], H. Ronald Kaback[b,c,d,1], and Daniel J. Müller[a,1]

[a]Department of Biosystems Science and Engineering, Eidgenössische Technische Hochschule Zürich, 4058 Basel, Switzerland; and Departments of [b]Physiology and [c]Microbiology, Immunology and Molecular Genetics, and [d]Molecular Biology Institute, University of California, Los Angeles, CA 90095

Contributed by H. Ronald Kaback, March 10, 2014 (sent for review February 12, 2014)

The lactose permease (LacY) of *Escherichia coli*, a paradigm for the major facilitator superfamily, catalyzes the coupled stoichiometric translocation of a galactopyranoside and an H^+ across the cytoplasmic membrane. To catalyze transport, LacY undergoes large conformational changes that allow alternating access of sugar- and H^+-binding sites to either side of the membrane. Despite strong evidence for an alternating access mechanism, it remains unclear how H^+- and sugar-binding trigger the cascade of interactions leading to alternating conformational states. Here we used dynamic single-molecule force spectroscopy to investigate how substrate binding induces this phenomenon. Galactoside binding strongly modifies kinetic, energetic, and mechanical properties of the N-terminal 6-helix bundle of LacY, whereas the C-terminal 6-helix bundle remains largely unaffected. Within the N-terminal 6-helix bundle, the properties of helix V, which contains residues critical for sugar binding, change most radically. Particularly, secondary structures forming the N-terminal domain exhibit mechanically brittle properties in the unbound state, but highly flexible conformations in the substrate-bound state with significantly increased lifetimes and energetic stability. Thus, sugar binding tunes the properties of the N-terminal domain to initiate galactoside/H^+ symport. In contrast to wild-type LacY, the properties of the conformationally restricted mutant Cys154→Gly do not change upon sugar binding. It is also observed that the single mutation of Cys154→Gly alters intramolecular interactions so that individual transmembrane helices manifest different properties. The results support a working model of LacY in which substrate binding induces alternating conformational states and provides insight into their specific kinetic, energetic, and mechanical properties.

atomic force microscopy | membrane | transport protein | membrane protein structure | membrane protein folding | membrane transport

The lactose permease of *Escherichia coli* (LacY) of the major facilitator superfamily (MFS) (1, 2) catalyzes the coupled stoichiometric translocation of a galactopyranoside and an H^+ (sugar/H^+ symport) (3–6). Uphill (i.e., active) symport of galactoside against a concentration gradient is achieved by transduction of free energy released from the downhill movement of H^+ with the electrochemical H^+ gradient ($\Delta\tilde{\mu}_{H^+}$; interior negative and/or alkaline). Conversely, because coupling between sugar and H^+ is obligatory, downhill galactoside transport from a high to a low sugar concentration is coupled to uphill H^+ transport with the generation of $\Delta\tilde{\mu}_{H}$+, the polarity of which depends upon the direction of the sugar concentration gradient (7–10).

LacY monomers reconstituted into proteoliposomes are functional (11, 12), and X-ray crystal structures reveal 12, mostly irregular, transmembrane α-helices organized into two pseudo-symmetrical 6-helix bundles surrounding a large interior hydrophilic cavity open to the cytoplasm (13–16). At the apex of the hydrophilic cavity, which is at the approximate middle of the molecule, the galactoside- and H^+-binding sites are located. Side chains important for sugar recognition are located in both the N- and the C-terminal 6-helix bundles, whereas those involved in H^+ binding are largely in the C-terminal 6-helix bundle. Most X-ray structures obtained thus far exhibit a tightly sealed periplasmic side with the sugar-binding site at the apex of the cavity and inaccessible from the periplasm and an open cytoplasmic side (an inward-facing conformation). LacY is structurally highly dynamic, and binding of a galactoside closes the deep inward-facing cavity with opening of a complementary outward-facing cavity (reviewed in refs. 17, 18). Therefore, transport involves a large conformational change that allows alternating access of sugar- and H^+-binding sites to either side of the cellular membrane, and a recent structure indicates that an occluded intermediate is involved (19). Although structural models of LacY provide insight into the conformational states involved in transport, a crystal structure represents a static structural snapshot, and therefore an understanding of how sugar binding triggers the cascade of events that results in dynamic alternating access remains unclear. Furthermore, because these interactions alter the physical properties of LacY (reviewed in ref. 9), the energetic, kinetic, and mechanical properties of LacY that fulfill different functional roles during transport remain to be characterized.

Atomic force microscopy (AFM)-based single-molecule force spectroscopy (SMFS) has been applied to localize and quantify interactions that stabilize structural elements of an increasing number of native membrane proteins (20–25). Because SMFS can be used with membrane proteins embedded in native or synthetic lipid membranes under physiological conditions, the method has been used to assess interactions that change upon substrate binding, insertion of mutations, and assembly or lipid composition of the membrane (26–35). Moreover, when operated in the dynamic mode, dynamic single-molecule force spectroscopy (DFS) localizes and quantifies the kinetic, energetic,

Significance

Lactose permease of *Escherichia coli* (LacY), a model for the major facilitator superfamily, catalyzes galactopyranoside/H^+ symport across the membrane by a mechanism in which large conformational changes expose the sugar-binding site in the middle of the molecule alternatively to either side of the membrane (an alternating access mechanism). Despite substantial progress with respect to static X-ray crystal structures of LacY, the dynamics of the transport mechanism are not fully understood. Here we use dynamic single-molecule force spectroscopy to quantify the structural properties that change upon substrate binding. The results reveal very significant changes in conformational, kinetic, energetic, and mechanical properties primarily in the N-terminal 6-helix bundle, while the C-terminal 6-helix bundle remains largely unaffected.

Author contributions: H.R.K. and D.J.M. designed research; T.S., J.S., S.K., and S.A.M. performed research; J.S. contributed new reagents/analytic tools; T.S., M.G.M., H.R.K., and D.J.M. analyzed data; and T.S., M.G.M., H.R.K., and D.J.M. wrote the paper.

The authors declare no conflict of interest.

[1]To whom correspondence may be addressed. E-mail: rkaback@mednet.ucla.edu or daniel.mueller@bsse.ethz.ch.

This article contains supporting information online at www.pnas.org/lookup/suppl/doi:10.1073/pnas.1404446111/-/DCSupplemental.

and mechanical properties of the structural elements in a membrane protein in a physiologically relevant environment (20, 21).

LacY binds galactopyranosides, and 4-nitrophenyl-α-D-galactopyranoside (αNPG) is among the lactose analogs with highest affinity (~30 μM) (36). In the absence of substrate, LacY preferentially occupies an inward-facing open conformation, and substrate binding causes closing of the inward-facing cavity with opening of a reciprocal outward-facing cavity (reviewed in refs. 17, 18) with an occluded intermediate conformation (19). To understand the structural perturbations and properties associated with these conformations, we describe here the conformational, kinetic, energetic, and mechanical properties of LacY in the apo state and how these properties change upon substrate binding. SMFS and DFS are used to characterize the properties of individual structural segments of LacY and to describe how these regions change properties upon galactoside binding. To understand further how a single point mutation alters LacY, the conformationally restricted LacY mutant C154G (37), which crystallized originally (13), was also investigated. All measurements were conducted with wild-type (WT) or mutant C154G LacY embedded in a phospholipid membrane under physiological conditions. The findings quantify the structural properties of WT LacY, which change drastically upon sugar binding. In contrast, the structural properties of mutant C154G LacY remain largely unaffected by ligand binding.

Results

SMFS of WT LacY. WT LacY was expressed, purified by metal-affinity chromatography (*SI Appendix*, Fig. S1*A*), and reconstituted into 1-palmitoyl-2-oleoyl-*sn*-glycero-3-phosphoethanolamine (POPE):1-palmitoyl-2-oleoyl-sn-glycero-3[phospho-rac-(1-glycerol) (POPG) (3:1, mol:mol) liposomes (38). Successful reconstitution was confirmed by AFM imaging (*SI Appendix*, Fig. S1 *B* and *C*). To conduct SMFS, we first localized proteoliposomes containing WT LacY by AFM and then pushed the AFM stylus onto the membrane with a force of ~1 nN for 0.5–1 s to attach the terminal polypeptides of LacY (*Materials and Methods*). Withdrawal of the AFM stylus mechanically stresses the polypeptide (Fig. 1*A*) and induces unfolding of LacY (21). Force–distance (FD) curves recorded upon withdrawal exhibit highly reproducible patterns (Fig. 1*B*). Theoretically, it is possible to mechanically pull and unfold LacY from either the N- or C-terminal end. To assign from which terminal the FD curves were recorded, we compared FD curves recorded from WT LacY with only a 6–His-tag C-terminal extension to those from WT LacY carrying a 36-amino-acid (aa) unstructured C-terminal "polyGly" extension [GSM(G_{11})EAVEEAVEEA(G_{11})S] followed by an 8-aa-long His-tag (*SI Appendix*, Fig. S1*A*; hereafter referred to as WT). Such sizable extensions of the C terminus do not influence the transport activity of LacY (39). FD curves recorded for polyGly WT LacY show the same unfolding force peak pattern as recorded for LacY with a His_6-tag except that the characteristic force peak pattern observed for polyGly WT LacY is shifted to ~40-aa-longer contour lengths (*SI Appendix*, Fig. S2). Therefore, WT LacY attaches predominantly to the AFM stylus via the C-terminal end. In addition, the initial force peaks detected at small distances between the AFM stylus and the membrane (0–15 nm) are masked by noise in the FD spectra of LacY with a His_6-tag, but clearly observed in the polyGly-tailed WT LacY. Furthermore, the elongated C-terminal end significantly increases the probability of attaching LacY to the AFM stylus from 0.01 to 0.1% (n = 2,974). Thus, WT LacY with the C-terminal extension is better suited for characterization by SMFS.

Having shown that LacY preferably attaches to the AFM stylus by the C-terminal end, ~1.4×10^6 FD curves were recorded to quantify the interactions of WT LacY from which ~0.1% showed a single LacY adhering to the AFM stylus (Fig. 2*A* and *SI Appendix*, Fig. S3). Superimposition of these FD curves recorded for WT LacY yields highly reproducible force peak patterns. These patterns can be interpreted as follows (20, 21): the retracting AFM cantilever stretches the C-terminal end and exerts a mechanical force on the protein. At sufficiently high force, the structural segment anchoring the C-terminal end unfolds, and the AFM cantilever relaxes. Further separation of the AFM stylus from the proteoliposome stretches the previously unfolded polypeptide until the next structural segment of LacY is released with a measured force. Each force peak in an FD curve (Fig. 2*A*) records the unfolding of a structural segment and detects the transition from one unfolding intermediate to the next. Accordingly, LacY unfolds step-by-step from the phospholipid bilayer via several highly reproducible unfolding intermediates. The magnitude of each force peak quantifies the strength of the interactions stabilizing the structural segment that unfolds when transiting from one unfolding intermediate to the next. It is also notable from previous SMFS experiments (20, 21, 40) and full atomistic molecular dynamics simulations (41–43) that similar FD patterns are observed when membrane proteins are mechanically pulled from either terminal, thereby indicating that the remaining intramembranous secondary structure elements remain arranged until they are removed in segments from the bilayer.

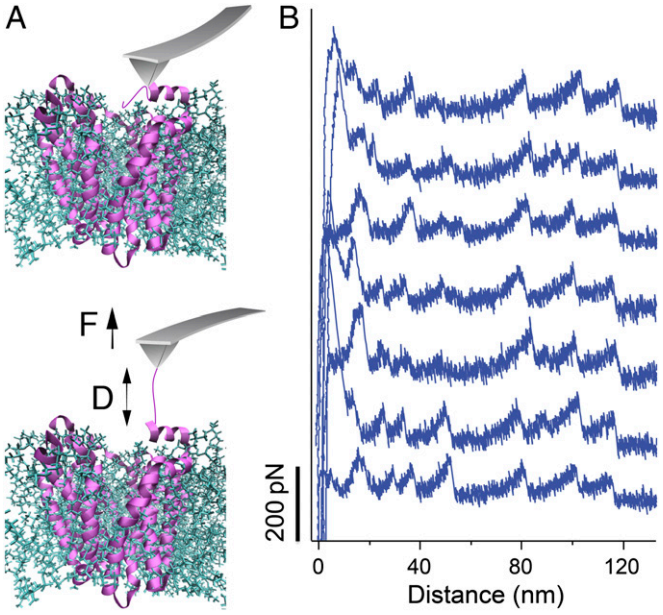

Fig. 1. SMFS of LacY reconstituted in POPE:POPG (3:1) phospholipid membranes. (*A*) Schematic representation of SMFS with LacY in a phospholipid bilayer. Upon pushing the AFM stylus onto the proteoliposome, the stylus adheres nonspecifically to the terminal end of the transporter. Withdrawal of the cantilever increases the distance *D* between the AFM stylus and the membrane. Consequently, the terminal end tethering the stylus stretches and a mechanical force, *F*, is applied to the transporter. Upon further withdrawal of the AFM stylus, the transporter begins to unfold stepwise. During this process, the FD curve is recorded. (*B*) Typical FD curves corresponding to mechanical unfolding of WT LacY from the C-terminal end. To increase the probability of attaching the C-terminal end to the AFM stylus, the C terminus of LacY was extended by 36 aa (polyGly) plus a His_8-tag (*SI Appendix*, Fig. S1). Although every FD curve shows unique features, all curves share common force peaks at specific stylus-sample distances. SMFS was performed in 50 mM KP_i (pH 7.2) at 25 °C. The cartoon in *A* shows the LacY structure (PDB ID code 1PV7) (13) prepared using visual molecular dynamics.

Structural Segments in the Absence and the Presence of Substrate. FD curves recorded upon unfolding WT LacY in the absence or presence of substrate (1 mM αNPG) reveal 10 characteristic force peaks (Fig. 2). Each force peak from each FD curve was

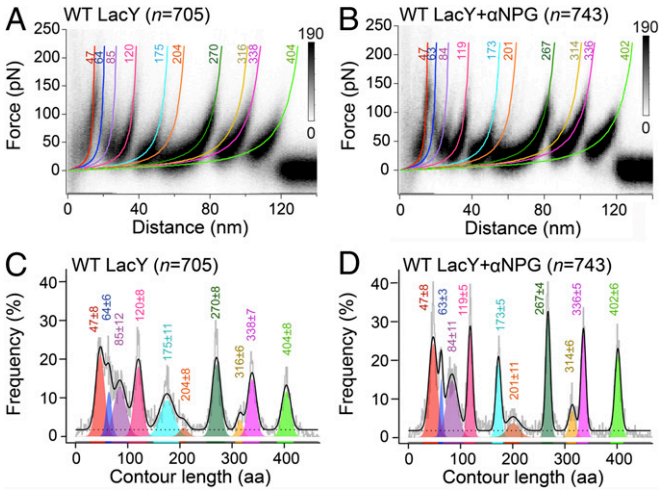

Fig. 2. Unfolding force peak patterns of WT LacY. Density plots of superimposed FD curves corresponding to the predominant force peak classes obtained upon mechanically unfolding WT LacY in the absence (*A*) and the presence (*B*) of αNPG. Colored curves represent WLC curves corresponding to the mean contour length of each force peak. Histograms of force peaks detected for WT LacY in the absence (*C*) and presence (*D*) of αNPG. Each probability density histogram was compiled after fitting every peak in every single FD curve using the WLC model. Colored Gaussian distributions give the mean contour length of each force peak class as obtained from fitting the histograms using the Gaussian mixture model. For each histogram, 10 force peak classes are determined. Each force peak class represents a weighted Gaussian model component highlighted by a unique color. Sums of weighted contour lengths for all force peaks (full mixture models) are shown by black solid lines (*C* and *D*). Dashed lines (*C* and *D*) represent the uniform baseline noise determined from *SI Appendix*, Eq. 2. The numbers at the top of each WLC curve and histogram peak represent the mean contour length in amino acids ±SD. Data from six pulling speeds (500, 700, 1,000, 3,000, 4,500, and 6,000 nm/s) are pooled (*SI Appendix*, Fig. S3). *n* is the number of FD curves superimposed (*A* and *B*) and analyzed (*C* and *D*). Experiments were performed in 50 mM of KP_i (pH 7.2) with or without 1 mM αNPG.

fitted using the worm-like-chain (WLC) model to reveal the contour length (in aa) of the unfolded, stretched LacY polypeptide (25, 44). Histograms showing the contour length at which the force peaks reproducibly occurred were generated (Fig. 2 *C* and *D*). To determine the mean contour lengths of the characteristic force peaks, all peaks from each histogram were simultaneously fitted using a Gaussian mixture model (35). The 10 characteristic force peaks recorded upon unfolding WT LacY from the elongated C-terminal end occur at mean contour lengths of 47, 64, 85, 120, 175, 204, 270, 316, 338, and 404 aa (Fig. 2*C*). The position of unfolding force peaks recorded for WT LacY in the presence and absence of αNPG were the same (Fig. 2 *C* and *D*) within the experimental error.

The mean contour lengths obtained from the force peak histograms were used to localize the interactions that stabilize structural segments of WT LacY (Fig. 3). The first force peak in an FD spectrum represents the unfolding of a structural segment and localizes the beginning of that unit. The subsequent force peaks localize the end of the previous stable segment and the beginning of the next stable segment. The mean contour lengths of the unfolding force peaks obtained from the force peak histogram (Fig. 2*C*) were used to determine the beginnings and ends of each structural unit in the secondary structure model obtained by linearizing the X-ray crystal structure (Fig. 3). To localize structural segments, counting begins from the C-terminal end from which LacY was unfolded (i.e., mirror image of the pulling distance/contour length shown in Fig. 2). To obtain location precisely, the length of C-terminal extension must be taken into account.

The structural segments of WT LacY read as following (Fig. 3): The first force peak at 47 aa represents structural segment S1 (red) established by the C terminus; the second force peak at 64 aa represents structural segment S2 (dark blue) established by the short periplasmic loop P6 and helix XII; force peak at 85 aa represents structural segment S3 (purple) established by helix XI; force peak at 120 aa represents structural segment S4 (magenta) established by loop C5, helix X, loop P5, and helix IX; force peak at 175 aa represents structural segment S5 (light blue) established by loop C4, helix VIII, and loop P4; force peak at 204 aa represents structural segment S6 (brown) established by the C-terminal half of loop C3 and helix VII; force peak at 270 aa represents structural segment S7 (dark green) established by the N-terminal half of loop C3, helix VI, loop P3, and periplasmic half of helix V; force peak at 316 aa represents structural segment S8 (yellow) established by the cytoplasmic half of helix IV, loop C2, and the cytoplasmic end of helix V; force peak at 338 aa represents structural segment S9 (violet) of the cytoplasmic end of helix II, loop C1, helix III, loop P2, and the periplasmic half of helix IV; and force peak at 404 aa represents structural segment S10 (pale green) of the N terminus, helix I, loop P1, and the periplasmic half of helix II. Because the unfolding force peaks of WT LacY are observed at the same positions in the absence and the presence of substrate (Fig. 2), it is apparent that substrate binding does not alter the structural segments (Fig. 3).

Energetic, Kinetic, and Mechanical Properties in the Absence and the Presence of Substrate. To further quantify the changes in WT LacY induced by substrate binding, DFS studies were carried out in the absence and presence of αNPG. DFS allows characterization of the unfolding free-energy landscape of each structural segment in LacY (Fig. 4) (21). Therefore, the kinetic, energetic, and mechanical property of each structural segment was quantified. For DFS, WT LacY was unfolded at six different pulling velocities (500, 700, 1,000, 3,000, 4,500, and 6,000 nm/s)

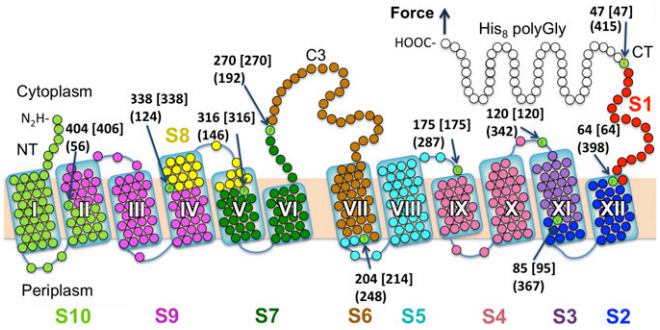

Fig. 3. Structural segments mapped to the secondary and tertiary structure model of WT LacY. Secondary structure model of LacY [derived from PDB ID code 1PV7 (13)] mapped with the 10 structural segments S1–S10. Each mean contour length of a force peak class of the force peak histograms (Fig. 2*C*) assigns the beginning of a structural segment (arrows pointing to aa). Black numbers at arrows indicate the mean contour lengths of a force peak class (in aa), numbers in square brackets indicate the aa position counted from the C-terminal end, and numbers in parentheses indicate the aa position from the N-terminal end. Each of these numbers assigns the end of the previous and the beginning of a new structural segment. To obtain their location, the length of polyGly linker and His-tag is taken into account. If the beginning/end of a stabilizing structural segment locates on the mica-facing side of the membrane or within the membrane, the thickness of the membrane is considered (69). Transmembrane helices are labeled I–XII; the middle cytoplasmic loop is labeled C3; N terminus, NT; C terminus, CT; and the unstructured C-terminal polyGly extension [GSM(G_{11})EAVEEAVEEA(G_{11})S] with the 8 His-tag His_8 polyGly.

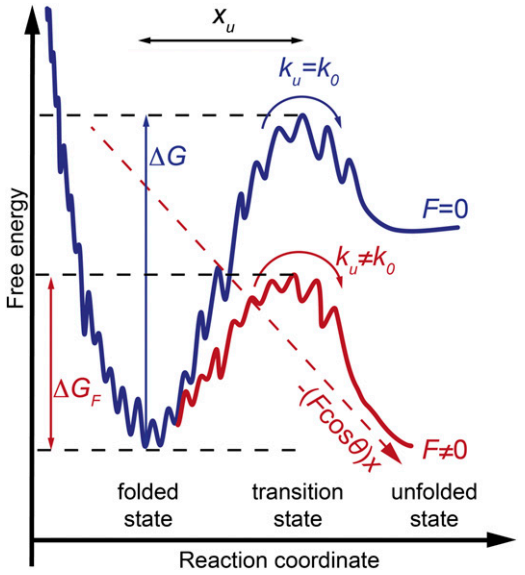

Fig. 4. Unfolding free-energy barrier characterizing the energetic (ΔG) and kinetic parameters (x_u, k_0) of the structural segments in LacY. According to the Bell–Evans model, a folded structure can be characterized by a two-state model (45, 47, 70). In the two-state model, the native folded state is stabilized by an energy valley and is separated from the unfolded state by a free-energy barrier. To induce unfolding of a stable structure segment, the transition state of the free-energy barrier has to be overcome. x_u is the distance between folded and transition state, k_0 the transition rate to cross the energy barrier in absence of an externally applied force (i.e., at thermal equilibrium), and ΔG the activation free energy needed to overcome the unfolding free-energy barrier. An externally applied force, F, changes the thermal likelihood of reaching the transition state of the unfolding free-energy barrier. The energy projection along the reaction coordinate (pulling direction of the externally applied force) is tilted by the applied mechanical energy $-F(\cos\Theta)x$ (red dashed line). "Θ" gives the angle between externally applied force and reaction coordinate. The tilt induced by the externally applied force decreases the free-energy barrier height (red curve) and increases the probability to overcome the transition state toward unfolding the structural segment.

(*SI Appendix*, Fig. S3). For each pulling velocity, the mean unfolding force of each reproducible force peak was analyzed over its contour length (*SI Appendix*, Figs. S4 and S5), and the mean unfolding forces were plotted over the loading rate (e.g., force applied over time) (*SI Appendix*, Fig. S6). Each DFS plot shows log-linear relationships between the unfolding force and the logarithmic loading rate, suggesting a two-state unfolding process by which a folded structural segment overcomes a single free-energy barrier toward unfolding (Fig. 4) (45–47). Linear regression was used for fitting the DFS plots, and the error propagation of the uncertainties was computed using Monte Carlo simulations (*SI Appendix*, Fig. S6) (35). This approach has the advantage of correctly accounting for nonlinearities and correlations among measurement errors. Fitting the DFS data to the Bell–Evans model (*SI Appendix*, Eq. 3) approximates the equilibrium unfolding rate k_0 in the absence of applied force and the distance separating the folded from the transition state x_u. The reciprocal of the unfolding rate k_0 describes the lifetime of a structural segment, whereas x_u approximates the width of the energy valley hosting the folded state. The number of conformational substates (i.e., conformational variability) hosted by an energy valley depends on this width. Hence, a structural segment characterized by a small x_u shows lower conformational variability than one having a larger x_u. Furthermore, using k_0 and x_u, the height of the unfolding free-energy barrier ΔG stabilizing a structural segment and the spring constant κ describing the mechanical rigidity of a structure were calculated (*SI Appendix*, Eqs. 4 and 5). These parameters were determined for every structural segment of WT LacY in the absence and presence of substrate and structurally mapped (Fig. 5 and *SI Appendix*, Table S1).

Transition-State Distances of Structural Segments. In the sugar-free state, the structural segments of WT LacY exhibit transition-state distances x_u ranging from 0.25 to 0.41 nm (Fig. 5 and *SI Appendix*, Table S1). Upon substrate binding to WT LacY, the x_u values of all structural segments significantly increase except for S1 formed by the C terminus and S2 by the transmembrane helix XII. The transition-state distance x_u of all other structural segments of WT LacY range from 0.48 to 1.24 nm, showing a 1.9- to 4.3-fold increase (Fig. 5). The highest increase in x_u upon substrate binding is found for structural segments S7, S8, S9, and S10 of the N-terminal domain and segment S6 of the C-terminal domain.

Lifetime of Structural Segments. The structural segments of the sugar-free state show transition rates k_0 ranging from 0.12 to 6.13 s^{-1} (Fig. 5 and *SI Appendix*, Table S1). A marked reduction of transition rates occurs upon substrate binding to WT LacY. Although every structural segment of WT LacY shows reduced transition rates upon substrate binding, all structural segments of the N-terminal domain (S7, S8, S9, and S10) and one segment (S6) of the C-terminal domain exhibit reduced transition rates to values of <0.01 s^{-1}. Consequently, these structural segments show the greatest increase in lifetime, changing several orders of magnitude.

Free Energy Barrier Heights of Structural Segments. Free energy barriers with ΔG ranging from 19 to 23 k_BT (Fig. 5 and *SI Appendix*, Table S1) flank the structural segments in the sugar-free state of WT LacY. Upon substrate binding, the structural segments significantly increase the magnitude of the free-energy barriers, which now range from 23 to 38 k_BT. This rather drastic free-energy increase is observed for all structural segments of the N-terminal domain (S7, S8, S9, and S10) and for some of the C-terminal domain (S3, S4, S5, and S6). However, the increase

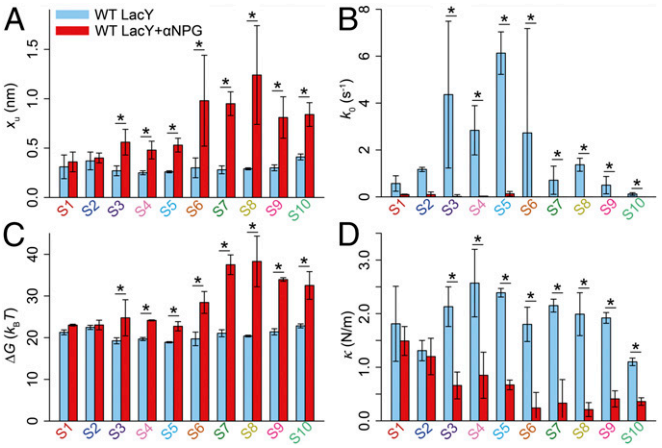

Fig. 5. Conformational, kinetic, energetic, and mechanical properties of WT LacY in the absence and presence of substrate. (*A*) Transition state distance x_u. (*B*) Transition rate k_0. (*C*) Height of the free-energy barrier ΔG. (*D*) Spring constant κ of every structural segment of WT LacY in the absence and presence of the substrate αNPG. The values revealed from analyzing the DFS data (*SI Appendix*, Figs. S3–S6) are in *SI Appendix*, Table S1. Differences between bound and unbound states are considered significant and highlighted by stars when P values approach <0.05 from the analysis of covariance (ANCOVA) test (*Materials and Methods*). Error bars represent SDs.

of the free-energy barrier heights in the N-terminal segments is much more pronounced ($\Delta\Delta G \sim 10$–$18\ k_BT$) compared with the segments of the C-terminal domain ($\Delta\Delta G \sim 3$–$8\ k_BT$). Among these changes, the largest increase of the free-energy barrier from ~20–21 k_BT to ~38 k_BT was observed for the structural segments S7 and S8, which share transmembrane helix V (Figs. 3 and 5).

Mechanical Properties of Structural Segments. The spring constant κ approximates the mechanical flexibility of a structural segment (21). In the absence of substrate, the structural segments of the WT display spring constants ranging from 1.10 to 2.57 N/m, with the average being 1.92 N/m (Fig. 5 and *SI Appendix*, Table S1). The mechanical properties of the WT change markedly upon substrate binding with the average spring constant of all structural segments decreasing by 77% to 0.64 N/m. This mechanical softening of WT LacY is most evident for the structural segments of the N-terminal domain. Among these the structural segments S7 and S8 containing transmembrane helix V increase flexibility by a factor of 6.5 and 9.5, respectively. In comparison, the structural segments S3, S4, and S5 of the C-terminal domain mechanically soften by a factor of ~3.2, whereas structural segment S6 softens by a factor of 7.5. Thus, upon substrate binding, the C-terminal domain of WT LacY increases flexibility as well, although at a lower magnitude on average relative to the structural segments of the N-terminal domain.

Structural Segments of Mutant C154G LacY. The conformationally constrained LacY mutant C154G binds ligand as well as, or better than, the WT but has minimal transport activity (37). Whereas sugar binding is mostly entropic with WT LacY, it is enthalpic with C154G LacY (48). Indeed, mutant C154G does not exhibit the long-range conformational changes observed on the periplasmic side upon ligand binding; it is thermostable with respect to ligand binding and aggregation (37) and is arrested in an open-outward conformation(s) in the membrane (49–52). However, the X-ray structure of conformationally restricted mutant C154G exhibits an open-inward conformation with a tightly sealed periplasmic side (13, 14). Because this conformation is the same as that observed for WT LacY (15), the observation indicates that crystallization selects a conformer of LacY that is not representative of the structure of the mutant in the membrane. Although evidence has been presented suggesting that the defect in mutant C154G may be due to closer packing between helices V and I (53, 54), the interactions that "stabilize" the outward-facing conformation in the mutant remain to be quantified. For this reason, we also decided to characterize mutant C154G LacY by SMFS in the absence and presence of substrate. The experimental conditions applied to quantify the interactions and properties stabilizing the mutant were identical to those applied to characterize the WT, including the unstructured polyGly extension extending the C-terminal end of mutant C154G LacY.

FD curves recorded by SMFS show 10 reproducible force peaks for C154G mutant (Fig. 6). As observed with the WT, the mean contour lengths of the force peaks do not depend on the presence of substrate within the experimental error. However, only 1 of the 10 force peaks of mutant C154G LacY shows a contour length different from the WT (Fig. 6). The force peak that differs is at 292 aa (yellow peak) for mutant C154G LacY (Fig. 6*A*), which is detected at 316 aa (yellow peak) for WT (Fig. 2*C*). When all of the structural segments of WT and mutant are mapped to the secondary structure of LacY (*SI Appendix*, Fig. S8 *A* and *B*), it is evident that the WT and the C154G mutant are composed of very similar structural units except for those associated with force peaks at 316 aa (for WT LacY) and at 292 aa (for mutant C154G LacY). With WT LacY, the force peak recorded at 316 aa indicates that the N-terminal half of loop C3,

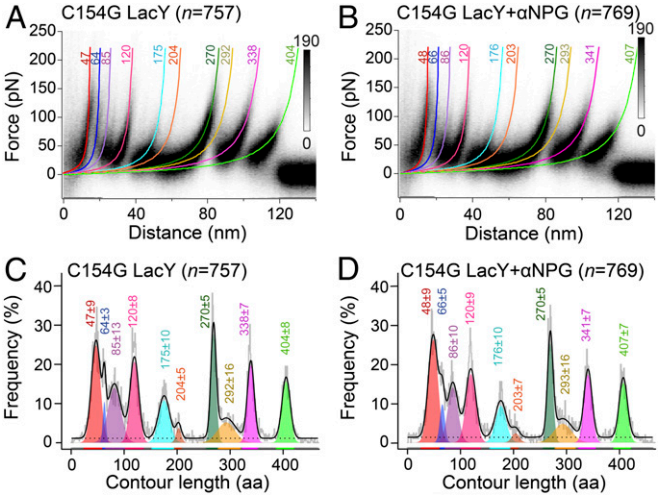

Fig. 6. Unfolding force peak patterns of mutant C154G LacY. Density plots of superimposed FD curves corresponding to the predominant force peak classes obtained upon mechanically unfolding mutant C154G in the (*A*) absence and (*B*) presence of αNPG. Colored curves represent WLC curves corresponding to the mean contour length of each force peak. Histograms of force peaks detected for mutant C154G LacY in the (*C*) absence and (*D*) presence of αNPG. Each histogram was compiled after fitting every peak in every single FD curve using the WLC model. Colored Gaussian distributions give the mean contour length of each force peak class as obtained from fitting the histograms using the Gaussian mixture model. For each histogram, 10 force peak classes are determined. Each force peak class represents a weighted Gaussian model component highlighted by a unique color. Sums of weighted contour lengths for all force peaks (full mixture models) are shown by black solid lines (*C* and *D*). Dashed lines (*C* and *D*) represent the uniform baseline noise. Numbers at the top of each WLC curve and histogram peaks represent the mean contour length in amino acids ±SD. Data from six pulling speeds (500, 700, 1,000, 3,000, 4,500, and 6,000 nm/s) are pooled (*SI Appendix*, Fig. S7). *n* is the number of FD curves superimposed (*A* and *B*) and analyzed (*C* and *D*). Experiments were performed in 50 mM of KP_i (pH 7.2) with or without 1 mM αNPG.

helix VI, the very short loop P3, and the periplasmic half of helix V establish a structural unit S7 (Fig. 3, dark green). The cytoplasmic end of helix V with the very short loop C2 and the cytoplasmic half of helix IV form another segment S8 (Fig. 3, yellow). In contrast, the shifted peak at 292 aa is represented by a different unit in mutant C154G (*SI Appendix*, Fig. S8). Helix VI together with loop P3 and the N-terminal half of loop C3 constitute structural segment S7* (dark green), and all of helix V forms stable segment S8* with loop C2 and the cytoplasmic half of helix IV (yellow).

Substrate Binding Does Not Alter the Properties of C154G LacY. To compare the kinetic, energetic, and mechanical properties of mutant LacY in the absence and the presence of substrate, DFS was conducted under identical experimental conditions as applied to WT LacY. Briefly, we recorded the FD spectra at different pulling velocities (*SI Appendix*, Fig. S7) and analyzed for each unfolding force peak the mean force, loading rate, and DFS plots (*SI Appendix*, Figs. S9–S11) to approximate energy landscape parameters (*SI Appendix*, Table S1). Compared with WT LacY in the unbound state, the structural segments of the C154G mutant show similar x_u values with minimal deviations. Upon substrate binding, the mutant significantly increases x_u for only structural segments S4 and S5 located at the C-terminal domain (Fig. 7). The increase in x_u for these two structural segments is much smaller (~1.1-fold) compared with the increase observed for the same (~1.9-fold) and other (up to 4.3-fold) structural segments of WT LacY in a substrate-bound state (Figs. 5 and 7).

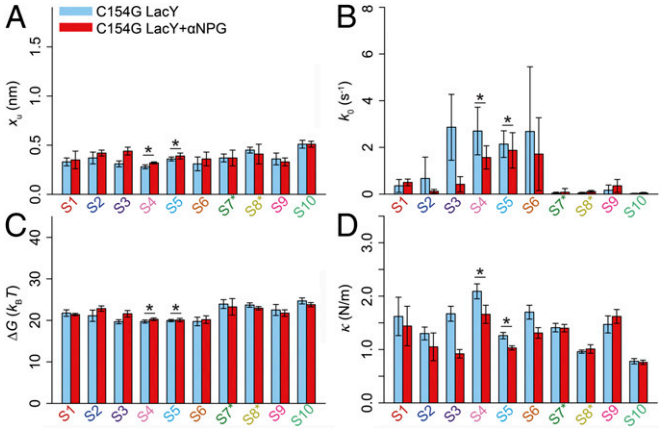

Fig. 7. Conformational, kinetic, energetic, and mechanical properties of mutant C154G LacY in the absence and presence of substrate. (*A*) Transition state distance x_u. (*B*) Transition rate k_0. (*C*) Height of the free-energy barrier ΔG. (*D*) Spring constant κ of every structural segment of WT LacY in the absence and presence of αNPG. The values revealed from analyzing the DFS data (*SI Appendix*, Figs. S7 and S9–S11) are in *SI Appendix*, Table S1. Differences between bound and unbound states are considered significant and highlighted by stars when *P* values approach <0.05 from the ANCOVA test (*Materials and Methods*). Error bars represent SDs.

In the unbound state, the structural segments of WT LacY show transition rates k_0 ranging from 0.12 to 6.13 s^{-1}, whereas segments of C154G LacY exhibit k_0 values from 0.02 to 2.86 s^{-1} (Fig. 7 and *SI Appendix*, Table S1). Because lifetime is reciprocal to the transition rate, it appears that the C154G mutation kinetically stabilizes the LacY structure. The largest differences are observed for the structural segments involving helix V, which hosts the C154G mutation. In WT LacY, structural segments S7 and S8 (Fig. 5) show transition rates of 0.71 and 1.37 s^{-1}, whereas, in the mutant the structural segments S7* and S8* (Fig. 7) with the same secondary structure, elements show transition rates of only ∼0.05 s^{-1}.

In the unbound state, free-energy barriers trap the structural segments of mutant C154G LacY with ΔG values ranging from 19 to 24 k_BT (Fig. 7). The differences of the free energy stabilizing the structural segments of WT LacY and mutant LacY are minor and range from ∼1 to 2 k_BT. Upon substrate binding, the structural segments of the mutant C154G barely change the height of their free-energy barriers (Fig. 7). Significant changes were observed only for structural segments S4 and S5 of the C-terminal domain. However, the free-energy changes in $\Delta\Delta G$ of these segments were <1 k_BT, 5- to 20-fold smaller relative to the free-energy changes observed for WT LacY upon substrate binding.

In the absence of substrate, the structural segments of mutant C154G LacY show mechanical spring constants ranging from 0.78 to 2.09 N/m (Fig. 7). The average spring constant of the C154G mutant (1.43 N/m) lies ∼25% below that determined for WT LacY (1.92 N/m). Most structural segments stabilizing the mutant do not change mechanical stiffness upon substrate binding. Only the S4 and S5 structural segments display any significant change in stiffness. These structural segments increase flexibility by the factor of ∼1.2, which is much less than the large increase in flexibility observed for WT LacY upon substrate binding, which ranges from 3- to 9.5-fold.

Discussion

Coordinated conformational transitions are fundamental to secondary transport and represent the basis for the alternating access mechanism. Binding of galactosides at the apex of the central cavity induces widespread conformational transitions, increasing the open probability of the hydrophilic cleft on the periplasmic side of the molecule, with closure of the cytoplasmic cavity in reciprocal fashion (17, 18). Hence, the catalytic cycle of the transporter does not rely on movement of sugar- or H^+-binding sites relative to the membrane. Rather, the protein essentially moves around the substrate, reciprocally exposing the binding sites to either side of the membrane [i.e., alternating access (55)]. X-ray structures of LacY, as well as other MFS transporters, give the impression that the conformational transitions occur as rigid body movements of the N- and C-terminal subdomains, but various biochemical and biophysical approaches provide converging evidence that LacY is in a highly dynamic state (56–58) and that it undergoes complex conformational changes that involve essential structural intermediates (9, 19, 59).

LacY adopts multiple conformational states with different probabilities in discrete transport modes (48). For example, in the ground state without substrate, LacY displays multiple intramolecular distances, which indicate conformational heterogeneity (18, 59). Thus, in addition to static structures of individual conformational states, it is essential to investigate the energetic, kinetic, and mechanical properties of these states, the intent of this work.

SMFS Reveals 10 Structural Segments in LacY. The 12 transmembrane helices within LacY are grouped into two 6-helix domains, which are related by twofold pseudosymmetry with an axis running perpendicular to the membrane and between the two halves (13). Further analysis reveals that the 6-helix domains themselves consist of two 3-helix bundles with an inverted topology, and it has been suggested that the conformational transitions resulting in alternating access involve conformational swaps between the 3-helix bundles (60).

SMFS detects reproducible force peak patterns for the WT and mutant C154G LacY (Figs. 2 and 6) consisting of 10 structural segments (Fig. 3). These segments consist of regions formed mostly by combinations of secondary structure elements made up of helices and loops, and the presence of substrate does not significantly alter the force peak patterns (Figs. 2 and 6). The diagnostic value of this observation is best summarized by the notion that substrate binding does not alter the spatial framework of the structural segments in LacY. This suggests that a mechanism involving opening and closing of isolated structural gates is unlikely with LacY, as those structural gates rely on spatially limited flexible hinge regions. Rather, changes in the position of large domains are consistent with preservation of the structural segments upon sugar binding.

Substrate Binding Drastically Changes Multiple Properties. The structural segments of WT LacY markedly change kinetic, energetic, and mechanical properties upon substrate binding. Among all structural segments in the WT, those constituting the N-terminal domain (helices I–VI) are more strongly affected than those of the C-terminal domain (helices VII–XII) (Figs. 5 and 8). In contrast, these parameters do not change significantly in mutant C154G upon substrate binding. In the following sections, the multiple alternations of kinetic, energetic, and mechanical properties of LacY upon sugar binding are discussed.

Lifetime. The transition rate k_0 describes the tendency of a structural segment to cross the free-energy barrier at thermal equilibrium (45, 46), whereas the reciprocal of k_0 describes the lifetime of the structural segment (lifetime = $1/k_0$). Substrate binding to WT LacY drastically reduces the transition rate k_0 and thus increases the lifetime of every structural segment (Figs. 5 and 8). Such a dramatic change in lifetime induced by substrate binding is not observed for other membrane proteins—including transporters—studied thus far (24, 30, 32, 35, 61). Fast transition rates between different states are intuitively indicative of facile energy landscapes and suggest a relaxed conformational ensemble (Fig. 9*A*).

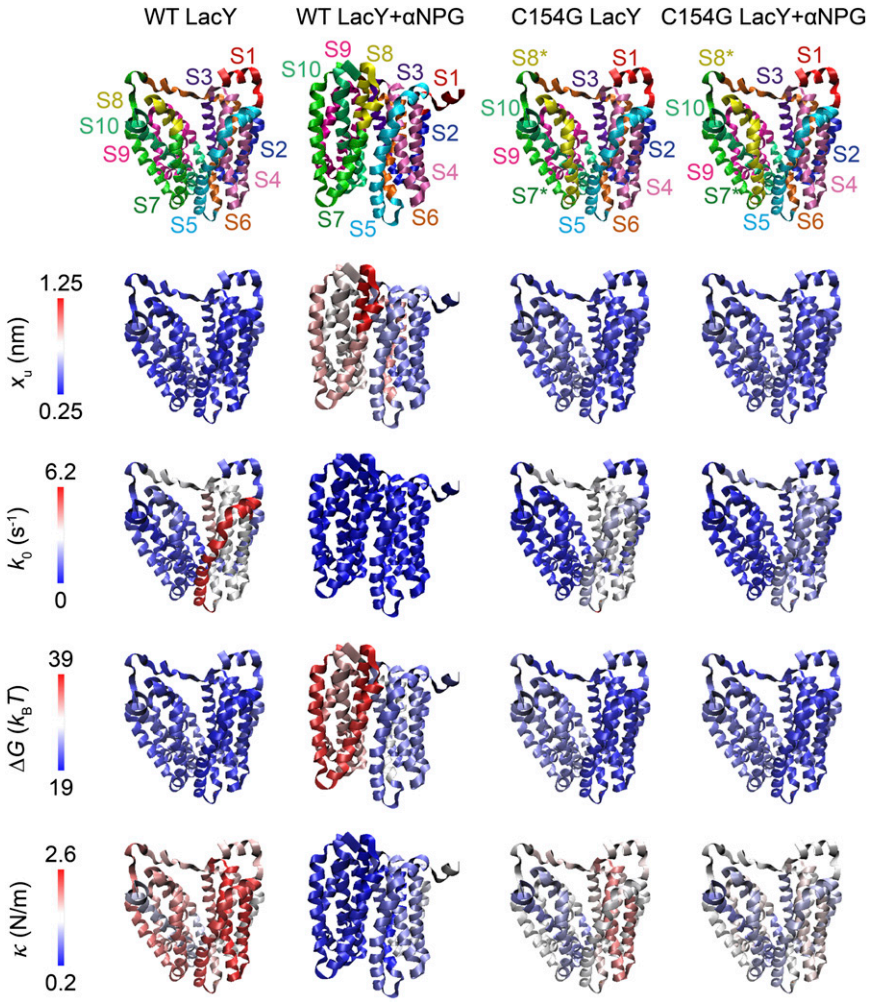

Fig. 8. Mapping the conformational, kinetic, energetic, and mechanical properties of WT and mutant C154G LacY in the absence and presence of substrate. Structural segments S1–S10 in LacY (Protein Data Bank ID code 1PV7) (13) are shown at the top row. Rows below map the transition-state distance x_u, transition rate k_0, the height of the free-energy barrier ΔG, and the spring constant κ of the structural segments in the absence and presence of the substrate αNPG. The colored LacY backbone roughly indicates the value for each parameter as indicated by the scale bars (values taken from *SI Appendix*, Table S1). In the substrate-bound state, most structural segments stabilizing WT LacY increase conformational variability (x_u), lifetime (reciprocal of k_0), and free-energy barrier ΔG and decrease the mechanical spring constant κ (e.g., mechanical rigidity). The largest changes of these parameters are observed in the N-terminal domain of WT LacY. In the unbound state, mutant C154G LacY shows different properties compared with WT LacY and barely changes properties upon substrate binding.

The presence of substrate radically changes this property of LacY, and the molecule oscillates more slowly between the respective states (Fig. 5*B*).

Mechanical flexibility. The spring constant κ approximates the mechanical flexibility of structural segments. In the absence of substrate, the mechanical stiffness of the structural segments in WT and mutant C154G LacY average 1.92 and 1.43 N/m, respectively. These values lie within those measured for structural segments stabilizing a variety of other membrane proteins (24, 30, 35, 62). Upon substrate binding the structural segments of WT LacY significantly increase flexibility (Fig. 9*B*). The most drastic softening is observed for structural segments S7, S8, and S9, which increase flexibility up to ∼9.5-fold to ≤0.41 N/m (Fig. 5*D*). However, structural segments S3, S4, and S5 of the C-terminal domain mechanically soften as well by a factor of ∼3, whereas S6 softens by a factor of ∼7.5. Thus, substrate binding increases the flexibility of the entire molecule with the greatest changes occurring in the N-terminal domain.

Conformational space. The transition-state distance x_u describes the width of the free-energy valley stabilizing a structural segment (Fig. 4). A wider free-energy valley can host more conformational substates of a structural segment. In the apo state, the structural segments in the WT display x_u values ranging from 0.25 to 0.41 nm (Fig. 5*A*). Comparison with x_u values for structural segments in other membrane proteins reveals that the x_u values determined for WT LacY in the substrate-free state are at the lower end of the values obtained for other membrane proteins [i.e., 0.15–0.69 nm for bacteriorhodopsin (62); 0.26–0.55 nm for the human β_2-adrenergic receptor (24); 0.26–0.50 nm for unliganded mouse opsin (35); 0.28–0.70 nm for the Na^+/H^+ antiporter NhaA (61); 0.21–0.36 nm for the apo amino acid transporter SteT (30)]. Thus, apo LacY occupies a relatively small conformational space with low conformational variability (Fig. 9*B*).

This situation changes dramatically upon substrate binding to WT LacY. The transition-state distance x_u of all structural segments increases 1.9- to 4.3-fold, except for the structural segments formed by the C terminus (S1) and transmembrane helix XII (S2) (Fig. 5*A*). Substrate binding induces increases in the transition-state distance, which greatly enhances the conformational variability of the structural segments and of LacY in general (Fig. 9*B*). This is consistent with results obtained by isothermal titration calorimetry (48). Thermodynamic characterization of ligand binding to WT LacY shows that substrate binding is primarily entropic. Based on this and other results it was concluded that sugar binding increases the number of conformational states that can be occupied by WT LacY.

Free energy. In apo WT LacY, the structural segments are trapped by free-energy barriers (ΔG) with heights ranging from 19 to 23 k_BT (Fig. 5*C*). These values are comparable to those observed for other membrane proteins. ΔG values measured for bacteriorhodopsin range from 20 to 29 k_BT (62), for the human β_2-adrenergic receptor from 17 to 21 k_BT (24), for unliganded mouse opsin from 21 to 25 k_BT (35), for NhaA from 22 to 30 k_BT (61), and for apo SteT from 15 to 18 k_BT (30). Thus, relatively normal free-energy barriers are present in apo WT LacY.

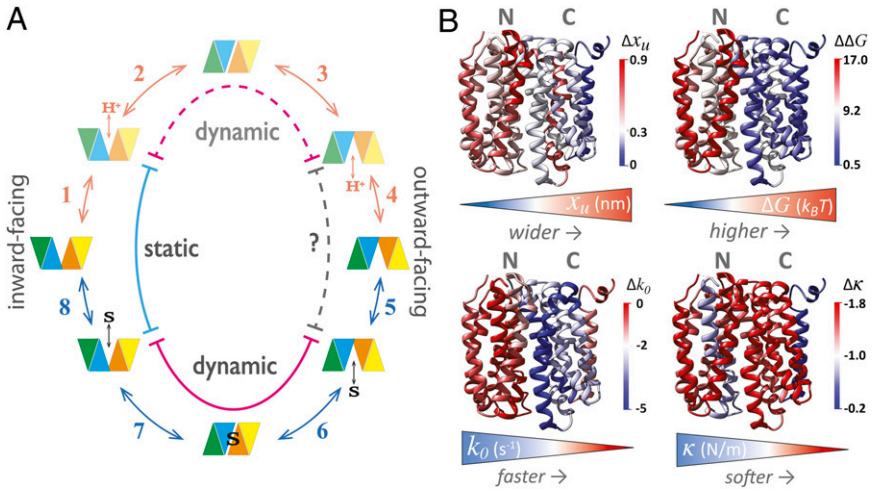

Fig. 9. Change of dynamic and structural properties upon sugar binding to LacY. (*A*) Overview of the postulated steps in the transport model. The direction of the green and blue triangles indicates the conformation of the N-terminal, and orange and yellow indicate the conformation of the C-terminal 6-helix bundle. Steps are numbered consecutively: the sequence starts from the inward-facing conformer; conformational transition of the apo-carrier is from inward-facing to outward-facing conformation (steps 1–4). Reorientation of LacY to a binding-competent state (step 5), binding of sugar and induced fit to the occluded intermediate (step 6); opening of the periplasmic cavity and release of sugar (step 7); conformational cycling of inward-facing conformations (steps 1 and 8). The red portion of the arrows indicates regeneration of the outward-facing cavity, and sugar transport is indicated by the blue portion of the arrows. All steps are reversible. The blue line in the cycle refers to a static conformational interval, and the solid magenta line refers to a dynamic conformational interval (the broken lines indicate conformational intervals inferred by symmetry). (*B*) Substrate-bound (PDB ID 4OAA, *Right*) structure of LacY colored according to the differences in given parameters relative to substrate-free LacY. The triangular color keys summarize the change in physical and mechanical properties changing upon sugar binding: transition-state distance x_u, lifetime (reciprocal of k_0), free-energy barrier ΔG, and mechanical spring constant κ (e.g., mechanical rigidity). The largest changes in these properties are observed in the N-terminal domain of WT LacY (*SI Appendix*, Table S1).

To transport sugar, high-energy barriers exist. Substrate binding shifts the N-terminal structural segments of LacY to a conformation flanked by high-energy barriers with values ranging from 23 to 38 k_BT (Fig. 5*C*). The largest free-energy increase by $\Delta\Delta G$ of ∼18 k_BT to a final value of ∼38 k_BT is observed for the structural segment S8, which contains Phe140 and Gly141, two side chains involved in a zipper-like motif that seals the cytoplasmic cavity in a sugar-bound occluded state (19). Overall, the DFS experiments demonstrate quantitatively that structural segments S7, S8, S9, and S10 of the N-terminal domain, which are involved in substrate binding, exhibit a large increase in ΔG (Fig. 9*B*).

Sequential Conformational Transition. The conformational, kinetic, energetic, and mechanical parameters determined by SMFS directly describe the structural properties of LacY changing upon substrate binding (Figs. 8 and 9). Strikingly, binding of sugar causes the N-terminal structural segments to assume a dynamic conformation with a broad variety of substates (increasing x_u values). This dynamic conformational ensemble of substates is kinetically and energetically stabilized by an increasing lifetime (decreasing k_0 values) and free-energy barrier (increasing ΔG values). The increase in mechanical flexibility of the N-terminal segments (decreasing κ-values) might release conformational restrains in the C-terminal 6-helix bundle, allowing relaxation into the static state with opening of the periplasmic cavity. Importantly, because the occluded state involves induced fit (19), it cannot be established without sugar binding. In other words, it is sugar binding that catalyzes the conformational transitions.

Crippled State of the C154G Mutant. As with WT LacY, the C154G mutant exhibits 10 structural segments (Fig. 6 and *SI Appendix*, Fig. S8). The structural segments overlap with the exception of the segment involving transmembrane helix V that carries the C154G mutation. In WT LacY, two structural segments contain helix V and are detected by the force peak observed at contour length 316 aa (position 146 aa in LacY) (Figs. 2 and 3). In the C154G mutant, this force peak is shifted to contour length 292 aa (position 161 aa in LacY) (Fig. 6 and *SI Appendix*, Fig. S8). The values of x_u, k_0, ΔG, and κ, which change dramatically upon sugar binding with WT LacY, do not display significant changes. It is indeed remarkable that this single mutation severely attenuates flexibility in LacY, apparently coinciding with the appearance of the new structural segment S8* composed of helix V, cytoplasmic loop C2, and the cytoplasmic end of helix IV.

The C154G mutation places a Gly residue in close proximity to a native Gly residue at position 24, thereby causing helices V and I to come into closer proximity where the helices cross in the middle of the membrane (13, 37, 53). This aberrant tighter interaction between helices I and V at the point of intersection is the probable cause for inactivation of LacY because replacement of Gly24 with Cys leads to restoration of activity (53). Moreover, cross-linking experiments demonstrate that a ligand-induced scissors-like movement between helices I and V near the point where the two helices cross is important for transport activity (54). Because helix V contains Arg144 and Trp151, which play a direct role in sugar binding (19), it seems reasonable to suggest that a sugar-induced conformational change(s) in helix V is then propagated through the remaining helices in LacY in a cooperative manner (63).

The experimental results presented here show that substrate binding to mutant C154G LacY barely changes the properties of the structural segments (Figs. 7 and 8). This observation is in stark contrast with the marked changes observed for the WT. The only two structural segments of C154G LacY that change properties significantly upon substrate binding are S4 and S5, which are located in the C-terminal domain. Interestingly, the trend by which substrate binding modifies the properties of structural segments in the mutant is similar to that observed for WT LacY (e.g., conformational variability, kinetic, and energetic stability increase, and the spring constant decreases). However, these changes quantified for the mutant are much smaller and are often insignificant compared with those observed for WT LacY.

Conclusions. X-ray or electron crystallography provides valuable insights into static structures. LacY and other MFS transporters have been crystallized in different conformations, which give the impression that symporters function via an alternating access mechanism that involves rigid body movements of the two 6-helix bundles comprising their structures (13, 63, 64). However, biochemical and biophysical techniques uniformly provide converging evidence for a highly dynamic nature for LacY. Even in a dormant state without a galactoside, LacY populates many different conformational substates (18, 48, 59). Thus, any given X-ray structure of LacY selects one conformer among many. Sugar transport by LacY involves large conformational changes that allow alternating access (17, 18, 65). An understanding of how sugar binding triggers the cascade of events resulting in dynamic alternating access remains unclear.

It has been postulated that sugar binding induces a lowering of the activation energy barrier for the transition between the inward-facing and outward-facing conformers of LacY and consequently expands the conformational space of the protein (59). Thus, LacY is proposed to operate in a very similar fashion to an enzyme, except that the intermediate is a conformer(s) of the symporter itself rather than a transition state intermediate of the substrate. In this regard, the recently solved structure of the LacY G46W/G262W (19) with a bound lactose analog provides support for an induced-fit mechanism for sugar binding and the alternating access mechanism in LacY. Accordingly, the fully ligated substrate interacts with residues from both the N- and C-terminal domains, and it seems very likely that these interactions provide the energy to approximate the two domains to form the occluded state.

These measurements complement this picture in several ways. First, a global increase in conformational flexibility of WT LacY upon ligand binding is observed. Second, an increase in the conformational variability of each structural segment upon sugar binding is observed and quantified. Third, the largest changes in kinetic, energetic, and mechanical properties upon sugar binding occur primarily in the N-terminal helix bundle of LacY. In addition, evidence suggesting that the alternating access mechanism may involve a sequential conformational change between the N- and C-terminal domains is presented.

Materials and Methods

Materials. Oligonucleotides were synthesized by Integrated DNA Technologies, Inc. Restriction enzymes were purchased from New England Biolabs. The QuikChange II kit was purchased from Stratagene. αNPG was purchased from Sigma. Talon superflow resin was purchased from BD Clontech. Dodecyl-β-D-maltopyranoside (DDM) and n-octyl-β-D-glucoside were from Anatrace, and synthetic phospholipids (POPE and POPG) were from Avanti Polar Lipids, Inc. All other materials were of reagent grade obtained from commercial sources.

Mutant Construction, Expression, and Purification. By using the QuikChange II PCR and plasmid pT7-5/LacY or pT7-5/mutant C154G as a template, a 36-aa "polyGly" followed by an 8-aa-long His-tag extension [GSM(G_{11})EAVEEAVEEA (Gly_{11})S(His_8)] was engineered onto the C terminus of LacY. WT LacY and mutant C154G were purified from *E. coli* XL1-Blue (Stratagene) transformed with pT7-5 plasmids harboring given mutant genes by using Co(II) affinity chromatography as described (53). Protein eluted from the Co(II)-Talon column was concentrated and washed with 50 mM NaP_i (pH 7.5)/0.01% DDM on an Amicon Ultra-15 concentrator with a 30K cutoff (Millipore). All protein preparations were at least 95% pure as judged by silver staining after SDS/PAGE. Samples with protein concentrations at 5–10 mg/mL in 50 mM sodium phosphate (NaP_i) buffer (pH 7.5)/2–4% wt/wt DDM were frozen in liquid nitrogen and stored at −80 °C.

Reconstitution of Purified Proteins into Proteoliposomes. Synthetic phospholipids (POPE/POPG; ratio 3:1) were used for protein reconstitution by the dilution method (38). Briefly, purified LacY in 0.02% wt/wt DDM was mixed with phospholipids dissolved in 1.2% wt/wt octyl-β-D-glucopyranoside at a lipid-to-protein ratio of 5 (wt/wt). The mixture was kept on ice for 20 min and then quickly diluted 50 times in 50 mM NaP_i (pH 7.5). The proteoliposomes were collected by centrifugation at 100,000 × *g* for 1 h and subjected to two cycles of freeze–thaw/sonication before use.

SMFS and DFS. Proteoliposomes containing densely packed LacY were adsorbed for 20 min to freshly cleaved mica in SMFS buffer [50 mM potassium phosphate (KP_i), pH 7.2] in absence or presence of 1 mM αNPG. SMFS buffer was prepared with nanopure water (≥18 MOhm/cm, PURE-LAB Ultra, ELGA LabWater) and reagents from Sigma with a purity grade ≥98.5%. After adsorption to freshly cleaved mica, weakly attached membrane patches were removed by several cycles of gentle rinsing of the sample with SMFS buffer (66). SMFS was performed at ∼25 °C with an 850-nm laser-equipped AFM (NanoWizard II, JPK Instruments). Si_3N_4 cantilevers (OMCL RC800PCA, Olympus) having a nominal spring constant of 0.05 N/m were calibrated in SMFS buffer solution using the equipartition theorem before and after each experiment (67). To minimize errors that may occur due to uncertainties in the cantilever spring constant calibration, LacY was unfolded using at least five different cantilevers for each pulling velocity. DFS was conducted at six different velocities of cantilever retraction (500, 700, 1,000, 3,000, 4,500, 6,000 nm/s). For high-frequency data acquisition at pulling velocities >1,000 nm/s, an external 16-bit data acquisition card (NI PCI-6221, National Instruments) was used.

SMFS Data Selection. Mechanically fully unfolded and stretched LacY (417 aa extended by a 36-aa long polyGly tail and an His_8-tag) approaches a contour length of ∼129 nm [length per amino acid is ∼0.36 nm (68)]. To ensure that LacY was mechanically fully unfolded from the terminal end, only FD curves showing force peak patterns extending to more than 110 nm were selected for analysis (20, 21).

SMFS Data Analysis. For details see *SI Appendix*, appendix 1.

Calculation of Energy Landscape Parameters and Mechanical Rigidity. For details see *SI Appendix*, appendix 2.

ACKNOWLEDGMENTS. We thank I. Smirnova for purifying and providing LacY and C. Bippes and J. Thoma for technical assistance and critical discussion of the manuscript. This work was supported by the Swiss National Science Foundation, the European Union Marie Curie Actions program through the Actuation and Characterization at the Single Bond Limit (ACRITAS) Initial Training Network (FP7-PEOPLE-2012-ITN, Project 317348), National Institutes of Health Grants DK51131, DK069463, and GM073210, and the US National Science Foundation Grant MCB-1129551 (to H.R.K.).

1. Saier MH, Jr. (2000) Families of transmembrane sugar transport proteins. *Mol Microbiol* 35(4):699–710.
2. Law CJ, Maloney PC, Wang DN (2008) Ins and outs of major facilitator superfamily antiporters. *Annu Rev Microbiol* 62:289–305.
3. West IC (1970) Lactose transport coupled to proton movements in Escherichia coli. *Biochem Biophys Res Commun* 41(3):655–661.
4. West IC, Mitchell P (1973) Stoicheiometry of lactose-H+ symport across the plasma membrane of Escherichia coli. *Biochem J* 132(3):587–592.
5. Patel L, Garcia ML, Kaback HR (1982) Direct measurement of lactose/proton symport in Escherichia coli membrane vesicles: Further evidence for the involvement of histidine residue(s). *Biochemistry* 21(23):5805–5810.
6. Ramos S, Kaback HR (1977) The relationship between the electrochemical proton gradient and active transport in Escherichia coli membrane vesicles. *Biochemistry* 16(5):854–859.
7. Garcia ML, Viitanen P, Foster DL, Kaback HR (1983) Mechanism of lactose translocation in proteoliposomes reconstituted with lac carrier protein purified from Escherichia coli. 1. Effect of pH and imposed membrane potential on efflux, exchange, and counterflow. *Biochemistry* 22(10):2524–2531.
8. Kaback HR, Sahin-Tóth M, Weinglass AB (2001) The kamikaze approach to membrane transport. *Nat Rev Mol Cell Biol* 2(8):610–620.
9. Guan L, Kaback HR (2006) Lessons from lactose permease. *Annu Rev Biophys Biomol Struct* 35:67–91.
10. Garcia-Celma JJ, Smirnova IN, Kaback HR, Fendler K (2009) Electrophysiological characterization of LacY. *Proc Natl Acad Sci USA* 106(18):7373–7378.
11. Newman MJ, Foster DL, Wilson TH, Kaback HR (1981) Purification and reconstitution of functional lactose carrier from Escherichia coli. *J Biol Chem* 256(22):11804–11808.
12. Costello MJ, et al. (1987) Purified lac permease and cytochrome o oxidase are functional as monomers. *J Biol Chem* 262(35):17072–17082.
13. Abramson J, et al. (2003) Structure and mechanism of the lactose permease of Escherichia coli. *Science* 301(5633):610–615.
14. Mirza O, Guan L, Verner G, Iwata S, Kaback HR (2006) Structural evidence for induced fit and a mechanism for sugar/H+ symport in LacY. *EMBO J* 25(6):1177–1183.

15. Guan L, Mirza O, Verner G, Iwata S, Kaback HR (2007) Structural determination of wild-type lactose permease. *Proc Natl Acad Sci USA* 104(39):15294–15298.
16. Chaptal V, et al. (2011) Crystal structure of lactose permease in complex with an affinity inactivator yields unique insight into sugar recognition. *Proc Natl Acad Sci USA* 108(23):9361–9366.
17. Kaback HR, Smirnova I, Kasho V, Nie Y, Zhou Y (2011) The alternating access transport mechanism in LacY. *J Membr Biol* 239(1–2):85–93.
18. Smirnova I, Kasho V, Kaback HR (2011) Lactose permease and the alternating access mechanism. *Biochemistry* 50(45):9684–9693.
19. Kumar H, et al. (2014) Structure of sugar-bound LacY. *Proc Natl Acad Sci USA* 111(5): 1784–1788.
20. Kedrov A, Janovjak H, Sapra KT, Müller DJ (2007) Deciphering molecular interactions of native membrane proteins by single-molecule force spectroscopy. *Annu Rev Biophys Biomol Struct* 36:233–260.
21. Bippes CA, Muller DJ (2011) High-resolution atomic force microscopy and spectroscopy of native membrane proteins. *Rep Prog Phys* 74:086601.
22. Bosshart PD, et al. (2012) The transmembrane protein KpOmpA anchoring the outer membrane of Klebsiella pneumoniae unfolds and refolds in response to tensile load. *Structure* 20(1):121–127.
23. Thoma J, Bosshart P, Pfreundschuh M, Müller DJ (2012) Out but not in: The large transmembrane β-barrel protein FhuA unfolds but cannot refold via β-hairpins. *Structure* 20(12):2185–2190.
24. Zocher M, Fung JJ, Kobilka BK, Müller DJ (2012) Ligand-specific interactions modulate kinetic, energetic, and mechanical properties of the human β2 adrenergic receptor. *Structure* 20(8):1391–1402.
25. Bippes CA, et al. (2013) Peptide transporter DtpA has two alternate conformations, one of which is promoted by inhibitor binding. *Proc Natl Acad Sci USA* 110(42): E3978–E3986.
26. Kedrov A, Krieg M, Ziegler C, Kuhlbrandt W, Muller DJ (2005) Locating ligand binding and activation of a single antiporter. *EMBO Rep* 6(7):668–674.
27. Park PS, et al. (2007) Stabilizing effect of Zn2+ in native bovine rhodopsin. *J Biol Chem* 282(15):11377–11385.
28. Cisneros DA, et al. (2008) Transducer binding establishes localized interactions to tune sensory rhodopsin II. *Structure* 16(8):1206–1213.
29. Sapra KT, Balasubramanian GP, Labudde D, Bowie JU, Muller DJ (2008) Point mutations in membrane proteins reshape energy landscape and populate different unfolding pathways. *J Mol Biol* 376(4):1076–1090.
30. Bippes CA, et al. (2009) Substrate binding tunes conformational flexibility and kinetic stability of an amino acid antiporter. *J Biol Chem* 284(28):18651–18663.
31. Damaghi M, et al. (2010) pH-Dependent interactions guide the folding and gate the transmembrane pore of the beta-barrel membrane protein OmpG. *J Mol Biol* 397(4): 878–882.
32. Kedrov A, et al. (2010) Probing the interactions of carboxy-atractyloside and atractyloside with the yeast mitochondrial ADP/ATP carrier. *Structure* 18(1):39–46.
33. Ge L, Perez C, Waclawska I, Ziegler C, Muller DJ (2011) Locating an extracellular K+-dependent interaction site that modulates betaine-binding of the Na+-coupled betaine symporter BetP. *Proc Natl Acad Sci USA* 108(43):E890–E898.
34. Zocher M, Zhang C, Rasmussen SG, Kobilka BK, Müller DJ (2012) Cholesterol increases kinetic, energetic, and mechanical stability of the human β2-adrenergic receptor. *Proc Natl Acad Sci USA* 109(50):E3463–E3472.
35. Kawamura S, et al. (2013) Kinetic, energetic, and mechanical differences between dark-state rhodopsin and opsin. *Structure* 21(3):426–437.
36. Sugihara J, Smirnova I, Kasho V, Kaback HR (2011) Sugar recognition by CscB and LacY. *Biochemistry* 50(51):11009–11014.
37. Smirnova IN, Kaback HR (2003) A mutation in the lactose permease of Escherichia coli that decreases conformational flexibility and increases protein stability. *Biochemistry* 42(10):3025–3031.
38. Viitanen P, Newman MJ, Foster DL, Wilson TH, Kaback HR (1986) Purification, reconstitution, and characterization of the lac permease of Escherichia coli. *Methods Enzymol* 125:429–452.
39. Consler TG, et al. (1993) Properties and purification of an active biotinylated lactose permease from Escherichia coli. *Proc Natl Acad Sci USA* 90(15):6934–6938.
40. Engel A, Gaub HE (2008) Structure and mechanics of membrane proteins. *Annu Rev Biochem* 77:127–148.
41. Seeber M, Fanelli F, Paci E, Caflisch A (2006) Sequential unfolding of individual helices of bacterioopsin observed in molecular dynamics simulations of extraction from the purple membrane. *Biophys J* 91(9):3276–3284.
42. Kappel C, Grubmüller H (2011) Velocity-dependent mechanical unfolding of bacteriorhodopsin is governed by a dynamic interaction network. *Biophys J* 100(4):1109–1119.
43. Hensen U, Müller DJ (2013) Mechanistic explanation of different unfolding behaviors observed for transmembrane and soluble β-barrel proteins. *Structure* 21(8):1317–1324.
44. Bustamante C, Marko JF, Siggia ED, Smith S (1994) Entropic elasticity of lambda-phage DNA. *Science* 265(5178):1599–1600.
45. Bell GI (1978) Models for the specific adhesion of cells to cells. *Science* 200(4342): 618–627.
46. Evans E, Ritchie K (1997) Dynamic strength of molecular adhesion bonds. *Biophys J* 72(4):1541–1555.
47. Evans E (2001) Probing the relation between force—lifetime—and chemistry in single molecular bonds. *Annu Rev Biophys Biomol Struct* 30:105–128.
48. Nie Y, Smirnova I, Kasho V, Kaback HR (2006) Energetics of ligand-induced conformational flexibility in the lactose permease of Escherichia coli. *J Biol Chem* 281(47): 35779–35784.
49. Smirnova I, et al. (2007) Sugar binding induces an outward facing conformation of LacY. *Proc Natl Acad Sci USA* 104(42):16504–16509.
50. Majumdar DS, et al. (2007) Single-molecule FRET reveals sugar-induced conformational dynamics in LacY. *Proc Natl Acad Sci USA* 104(31):12640–12645.
51. Nie Y, Sabetfard FE, Kaback HR (2008) The Cys154→Gly mutation in LacY causes constitutive opening of the hydrophilic periplasmic pathway. *J Mol Biol* 379(4): 695–703.
52. Jiang X, Driessen AJ, Feringa BL, Kaback HR (2013) The periplasmic cavity of LacY mutant Cys154→Gly: How open is open? *Biochemistry* 52(37):6568–6574.
53. Ermolova NV, Smirnova IN, Kasho VN, Kaback HR (2005) Interhelical packing modulates conformational flexibility in the lactose permease of Escherichia coli. *Biochemistry* 44(21):7669–7677.
54. Zhou Y, Madej MG, Guan L, Nie Y, Kaback HR (2011) An early event in the transport mechanism of LacY protein: Interaction between helices V and I. *J Biol Chem* 286(35): 30415–30422.
55. Mitchell P (1957) A general theory of membrane transport from studies of bacteria. *Nature* 180(4577):134–136.
56. le Coutre J, Kaback HR, Patel CK, Heginbotham L, Miller C (1998) Fourier transform infrared spectroscopy reveals a rigid alpha-helical assembly for the tetrameric Streptomyces lividans K+ channel. *Proc Natl Acad Sci USA* 95(11):6114–6117.
57. Patzlaff JS, Moeller JA, Barry BA, Brooker RJ (1998) Fourier transform infrared analysis of purified lactose permease: A monodisperse lactose permease preparation is stably folded, alpha-helical, and highly accessible to deuterium exchange. *Biochemistry* 37(44):15363–15375.
58. Sayeed WM, Baenziger JE (2009) Structural characterization of the osmosensor ProP. *Biochim Biophys Acta* 1788(5):1108–1115.
59. Madej MG, Soro SN, Kaback HR (2012) Apo-intermediate in the transport cycle of lactose permease (LacY). *Proc Natl Acad Sci USA* 109(44):E2970–E2978.
60. Radestock S, Forrest LR (2011) The alternating-access mechanism of MFS transporters arises from inverted-topology repeats. *J Mol Biol* 407(5):698–715.
61. Kedrov A, Appel M, Baumann H, Ziegler C, Muller DJ (2008) Examining the dynamic energy landscape of an antiporter upon inhibitor binding. *J Mol Biol* 375(5):1258–1266.
62. Sapra KT, Park PS, Palczewski K, Muller DJ (2008) Mechanical properties of bovine rhodopsin and bacteriorhodopsin: Possible roles in folding and function. *Langmuir* 24(4):1330–1337.
63. Quistgaard EM, Löw C, Moberg P, Trésaugues L, Nordlund P (2013) Structural basis for substrate transport in the GLUT-homology family of monosaccharide transporters. *Nat Struct Mol Biol* 20(6):766–768.
64. Iancu CV, Zamoon J, Woo SB, Aleshin A, Choe JY (2013) Crystal structure of a glucose/H+ symporter and its mechanism of action. *Proc Natl Acad Sci USA* 110(44):17862–17867.
65. Madej MG, Kaback HR (2014) The life and times of Lac permease: Crystals ain't everything, but they certainly do help: To structure and beyond. *Membrane Transport Mechanism*, eds Ziegler C, Krämer R (Springer, Berlin), Vol 17, pp 121–159.
66. Müller DJ, Engel A (2007) Atomic force microscopy and spectroscopy of native membrane proteins. *Nat Protoc* 2(9):2191–2197.
67. Butt HJ, Jaschke M (1995) Calculation of thermal noise in atomic-force microscopy. *Nanotechnology* 6(1):1–7.
68. Rief M, Gautel M, Oesterhelt F, Fernandez JM, Gaub HE (1997) Reversible unfolding of individual titin immunoglobulin domains by AFM. *Science* 276(5315):1109–1112.
69. Müller DJ, et al. (2002) Stability of bacteriorhodopsin alpha-helices and loops analyzed by single-molecule force spectroscopy. *Biophys J* 83(6):3578–3588.
70. Evans E (1998) Energy landscapes of biomolecular adhesion and receptor anchoring at interfaces explored with dynamic force spectroscopy. *Faraday Discuss* 1–16.

Supplementary Information

Substrate-induced changes in the structural properties of LacY

Tetiana Serdiuk[a], M. Gregor Madej[b], Junichi Sugihara[b], Shiho Kawamura[a], Stefania Mari[a], H. Ronald Kaback[b,c,d,1], and Daniel J. Müller[a,1]

[a]Department of Biosystems Science and Engineering, Eidgenössische Technische Hochschule Zürich, 4058 Basel, Switzerland; [b]Departments of Physiology and [c] Microbiology, Immunology & Molecular Genetics; [d]Molecular Biology Institute, University of California, Los Angeles, CA 90095, USA

Running title: Single-molecule force spectroscopy of LacY

Classification: BIOLOGICAL SCIENCES, Biophysics and Computational Biology

Keywords: atomic force microscopy | transport protein | membrane protein structure | conformational change | sugar binding

[1] To whom correspondence may be addressed. Email daniel.mueller@bsse.ethz.ch or rkaback@mednet.ucla.edu

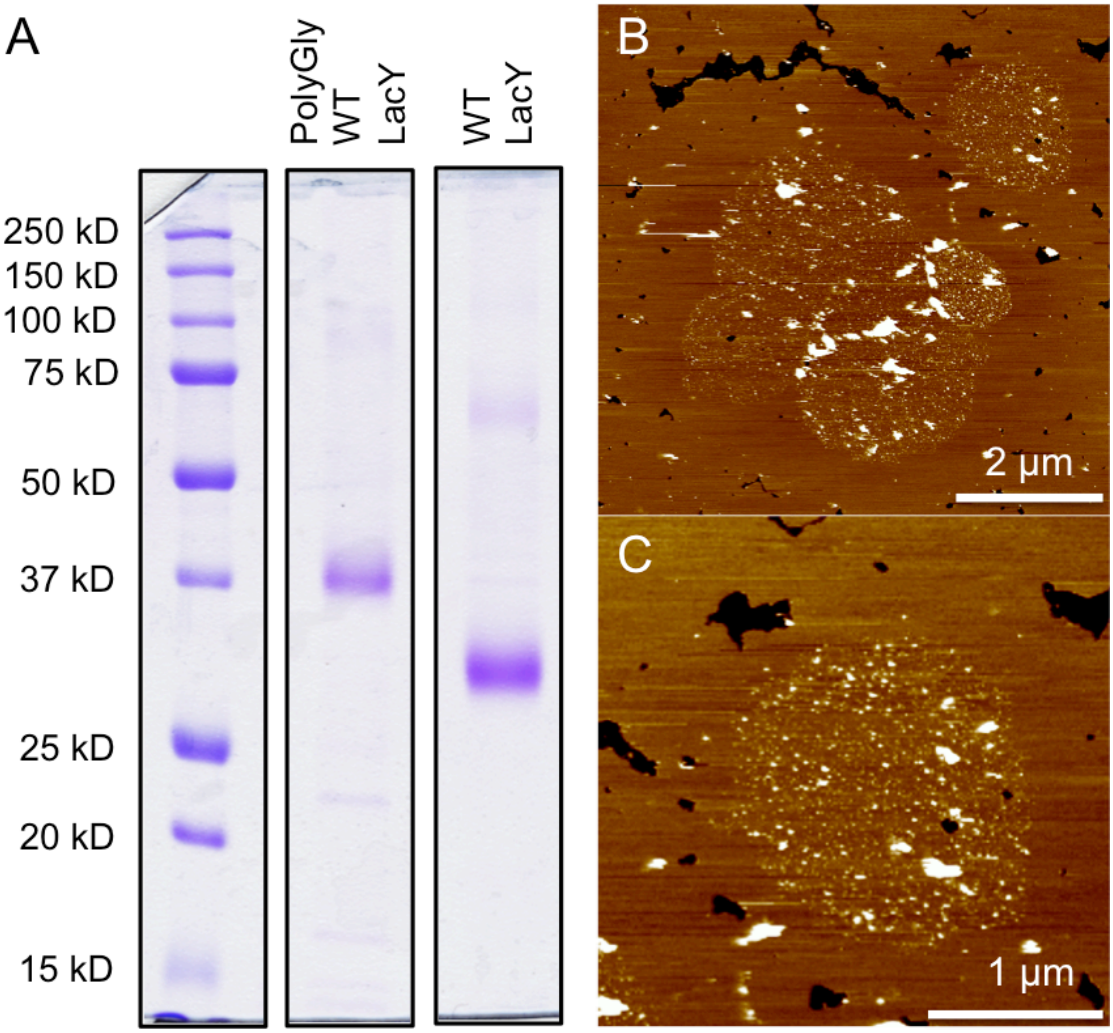

Fig. S1. Cloned, purified and reconstituted WT LacY. (***A***) SDS gel (acrylamide concentration is 12%) of purified LacY in proteoliposomes. The C-terminal end of wild-type (**WT**) LacY is either functionalized by a 6 aa long His-tag (**WT LacY**) or elongated by a 36 amino acid (**aa**) long polyglycine (**polyGly**) tail [GSM(G_{11})EAVEEAVEEA(G_{11})S] followed by 8 aa long His-tag (**polyGly WT LacY**). (***B***) Overview AFM topograph of polyGly WT LacY reconstituted into POPE:POPG (3:1, mol:mol) liposomes. The lipid membranes protrude 4.0 ± 0.3 nm (average ± SD; *n*=21) from the supporting mica surface. Thus, it can be concluded that upon adsorption to the support (mica) the LacY proteoliposomes open and adsorb as single layered membrane patches. (***C***) At higher magnification AFM topographs reveal LacY assemblies protruding from 1.7 ± 0.5 nm (*n*=24) the lipid surface. AFM topographs were recorded using contact mode AFM in buffer solution (200 mM KCl, 20 mM Hepes, pH 7.4) as described (1).

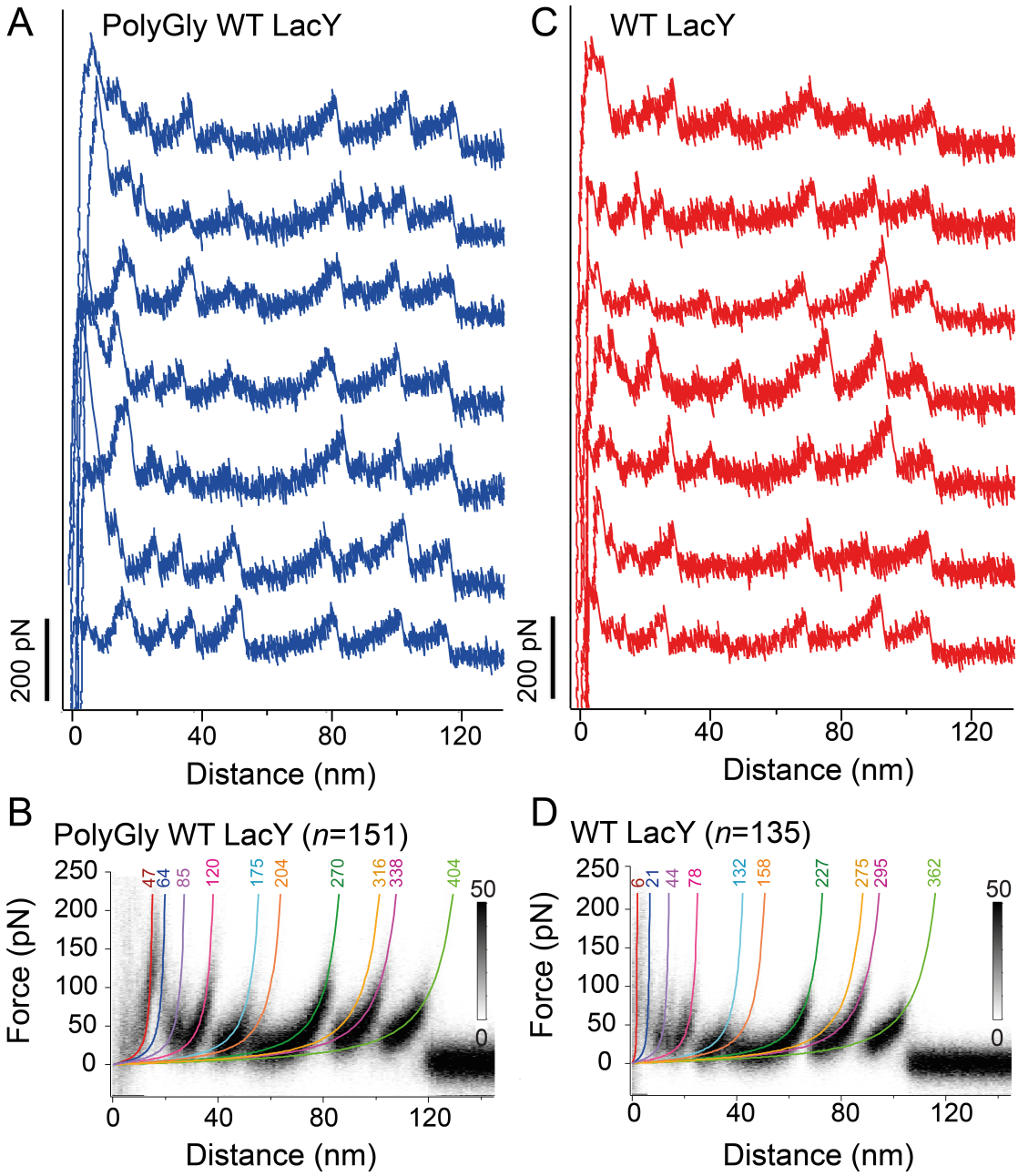

Fig. S2. SMFS of polyGly WT LacY and WT LacY reconstituted into POPE:POPG (3:1) liposomes. FD curves were recorded either upon mechanically unfolding C-terminally elongated WT LacY (polyGly WT LacY, (***A***)) or WT LacY (***B***). (***C,D***) Density plot of superimposed FD curves recorded upon unfolding polyGly WT LacY (**C**) and WT LacY (***D***). *n* gives the number of FD curves superimposed. Colored lines in (***C,D***) represent WLC curves fitting the mean contour length of individual force peaks. Compared to WT LacY, the WLC curves fitting the force peaks detected for polyGly WT LacY revealed ≈40 aa longer contour lengths. This shift corresponds to the ≈38 aa longer polyGly and His_8-tag elongating the C-terminal end (see **Fig. S1**). Accordingly, the FD curves recorded for polyGly WT LacY and WT LacY describe the mechanical unfolding from the C-terminal end. Note that unfolding PolyGly WT LacY detects the first unfolding force peak at a distance of ≈10–15 nm corresponding to a contour length of 47 aa (red colored WLC curve). In contrast, unfolding WT LacY without having an elongated C-terminal hardly reveals this unfolding force peak, which is masked by unspecific interactions occurring when the AFM tip and the protein membrane surface are in close proximity (<15 nm) (2, 3).

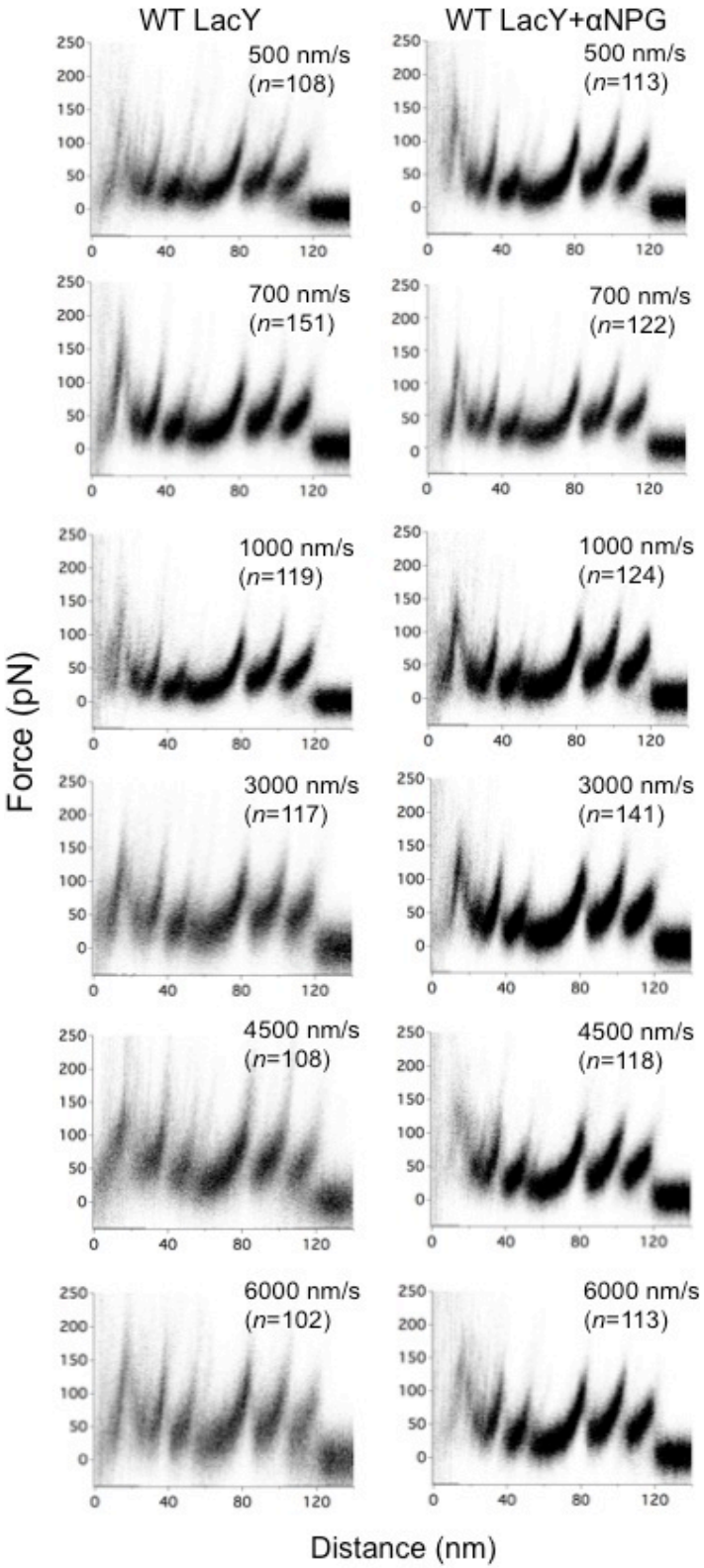

Fig. S3. Superimposed F-D curves recorded on unfolding of WT LacY reconstituted into POPE:POPG (3:1) liposomes and in the absence and presence of substrate (αNPG). Superimposed F-D curves are displayed as density plots. Pulling velocities and numbers (*n*) of superimposed F-D curves are indicated. F-D curves are aligned at three prominent force peaks detected at contour lengths of 270 aa, 338 aa, and 404 aa. The full gray scale corresponds to 50 counts. Data were recorded in buffer solution (50 mM KP_i, without or with 1 mM αNPG, pH 7.2) and at room temperature ≈25°C.

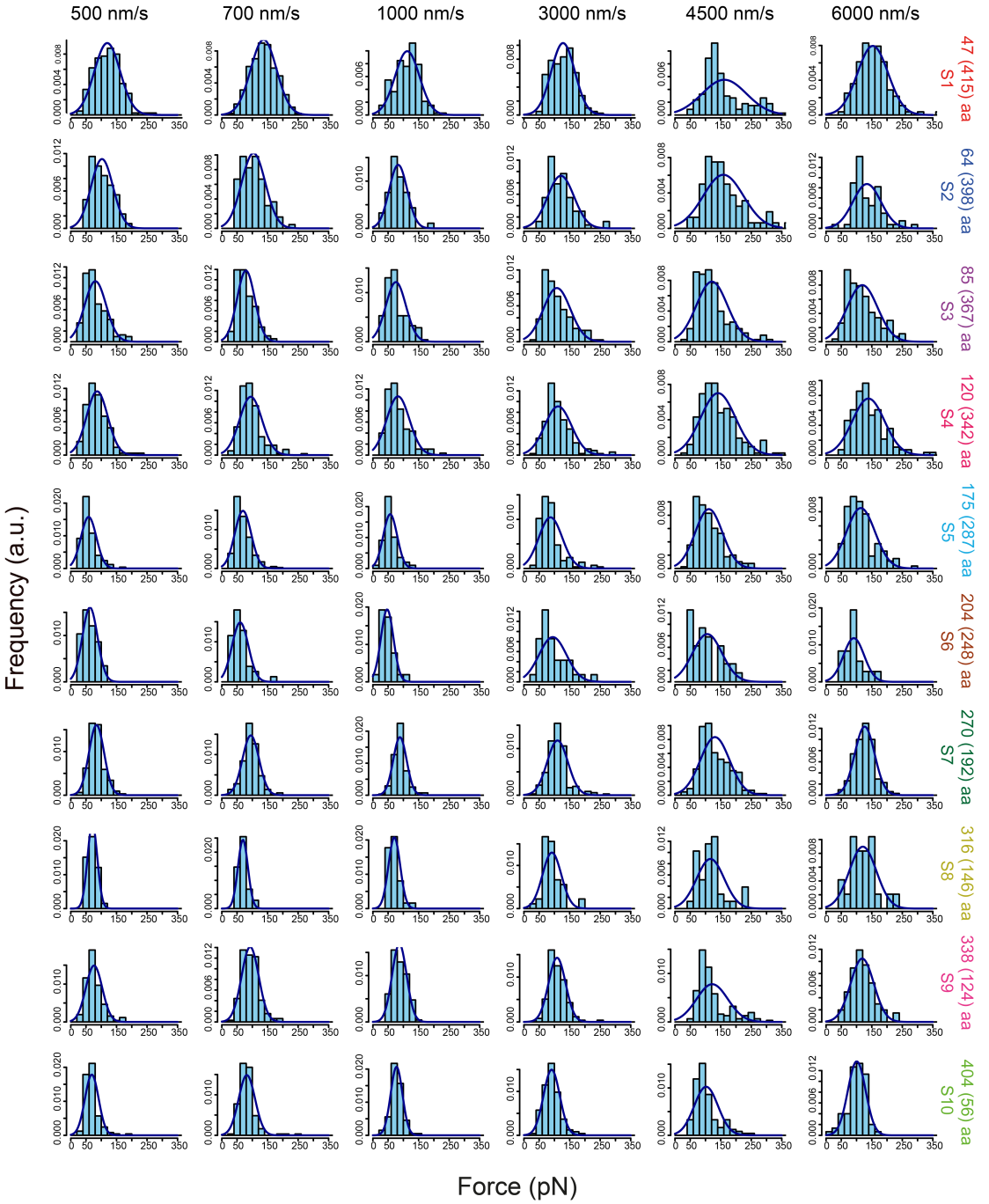

Fig. S4. Forces of unfolding force peaks recorded upon unfolding of WT LacY in the absence of substrate. Histograms show the force distribution of every unfolding force peak recorded for six different pulling velocities (500, 700, 1000, 3000, 4500, and 6000 nm/s). Colored numbers on the right side give mean contour lengths (in aa) obtained by fitting the force peak classes from contour length histograms (comp. **Fig. 2**), numbers in parentheses give the amino acid position at which a stable structural segment (labeled S1-S10) starts in LacY. The bin size of all histograms is 20 pN. Dark blue lines are Gaussian fits of force distributions. The DFS data is revealed analyzing the FD curves shown in **Fig. S3**.

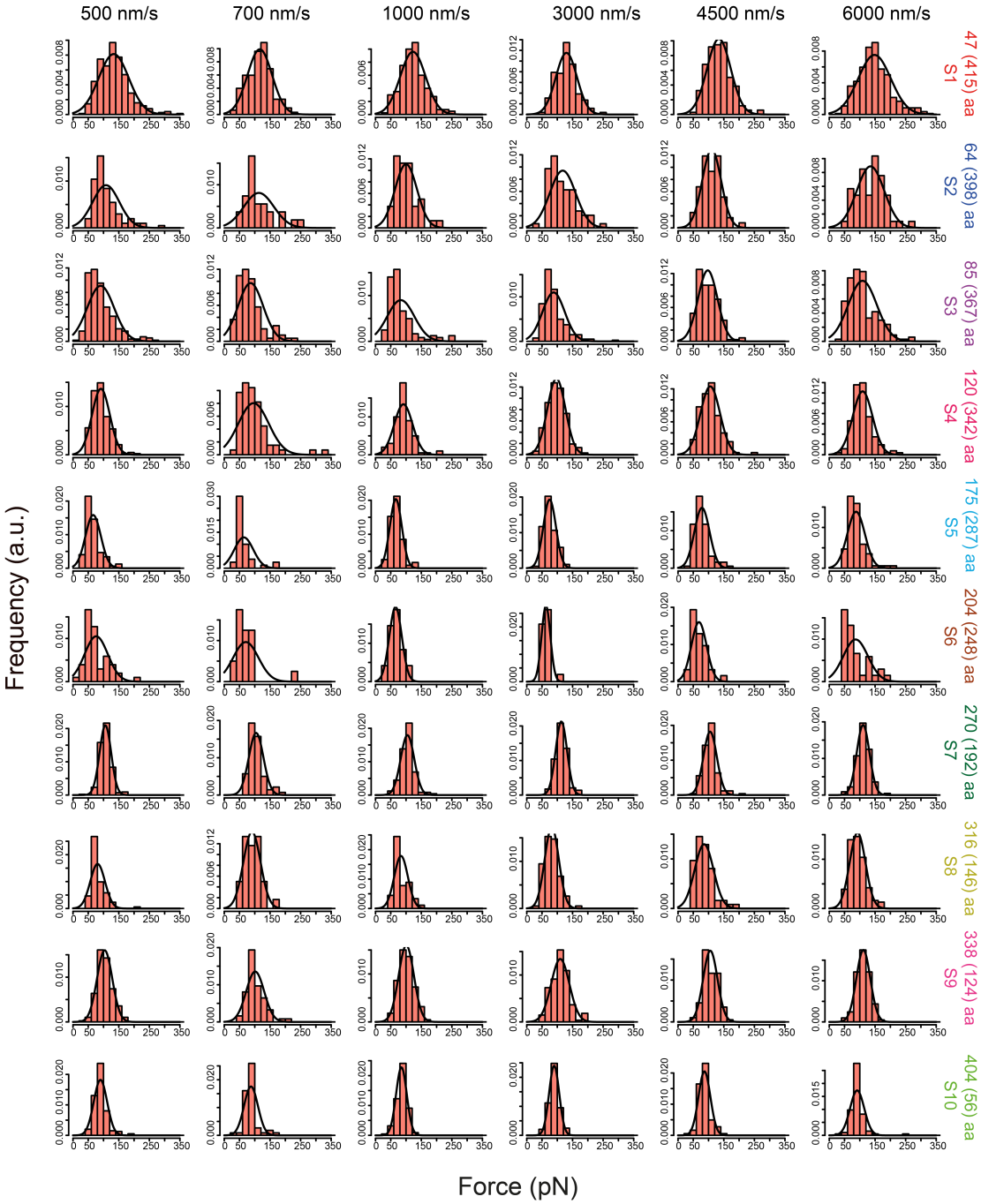

Fig. S5. Forces of unfolding force peaks recorded upon unfolding of WT LacY in the presence of substrate (αNPG). Histograms show the force distribution of every unfolding force peak recorded for six different pulling velocities (500, 700, 1000, 3000, 4500, and 6000 nm/s). Colored numbers on the right side give mean contour lengths (in aa) obtained by fitting the force peak classes from contour length histograms (comp. **Fig. 2**), numbers in parentheses give the amino acid position at which a stable structural segment (labeled S1-S10) starts in LacY. The bin size of all histograms is 20 pN. Dark blue lines are Gaussian fits of force distributions. The DFS data is revealed analyzing the FD curves shown in **Fig. S3**.

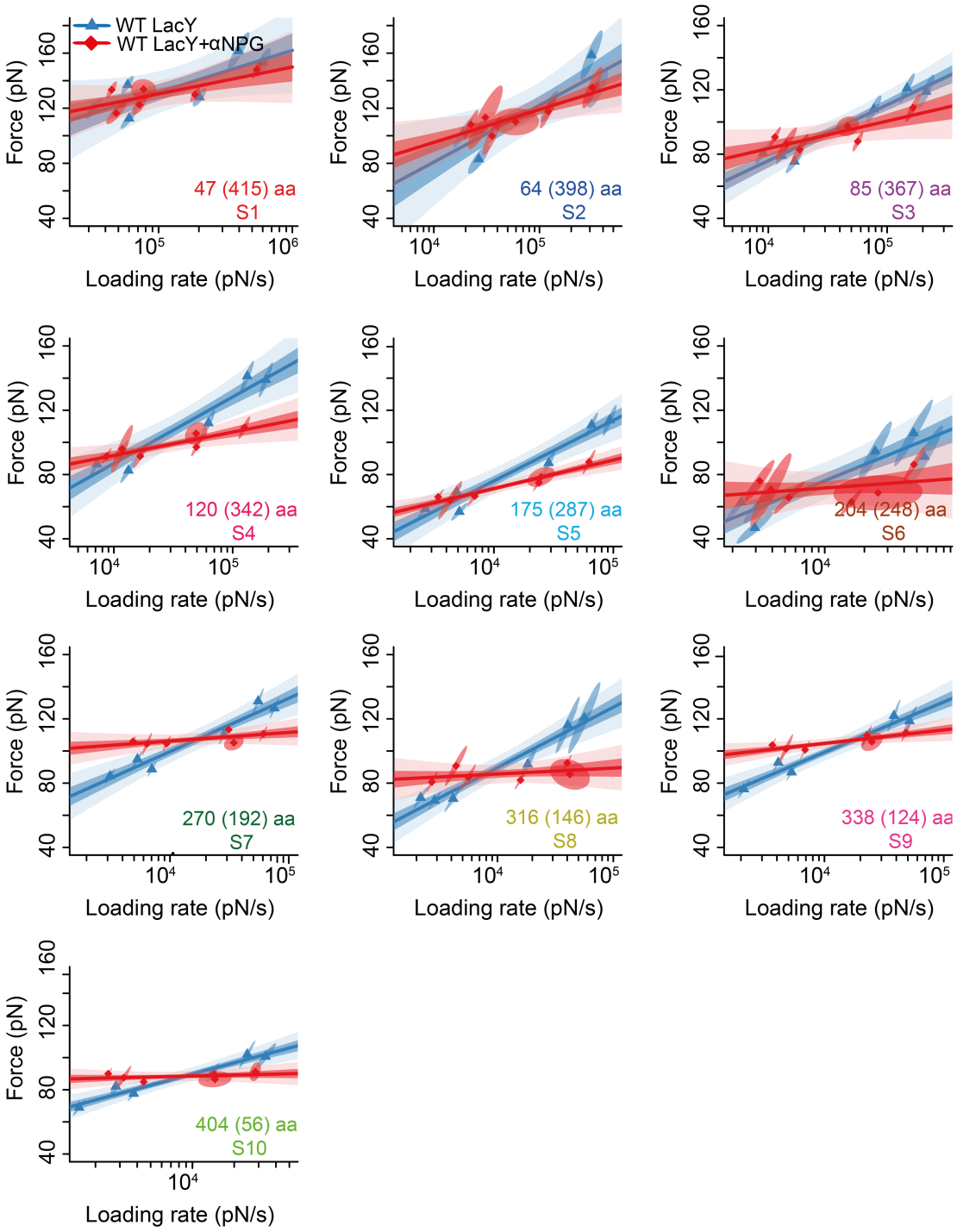

Fig. S6. Substrate binding modulates the interactions stabilizing the structural segments of WT LacY. Shown are DFS plots of each structural segment stabilizing of WT LacY reconstituted into liposomes. Colored numbers in each graph give mean contour lengths (in aa) obtained by fitting the force peak classes from contour length histograms (comp. **Fig. 2**), numbers in parentheses give the amino acid position at which a stable structural segment (labeled S1-S10) starts in LacY. Each DFS plot describes the dynamic behavior of a stable structural segment in the absence (blue) and in the presence (red) of the substrate αNPG. Plotted is the mean unfolding force of each stable structural segment *versus* the mean loading rate. Slanted ellipses indicate one standard error of each data point. The Bell-Evans model is fitted (solid lines) to the DFS plots to obtain the unfolding energy barrier parameters (Methods; **Equations 3 and 4**). Dark- and light-colored regions indicate fitting confidence intervals of one (68%) and two (95%) standard deviations, respectively. The DFS data is obtained analyzing the FD curves shown in **Fig. S3**.

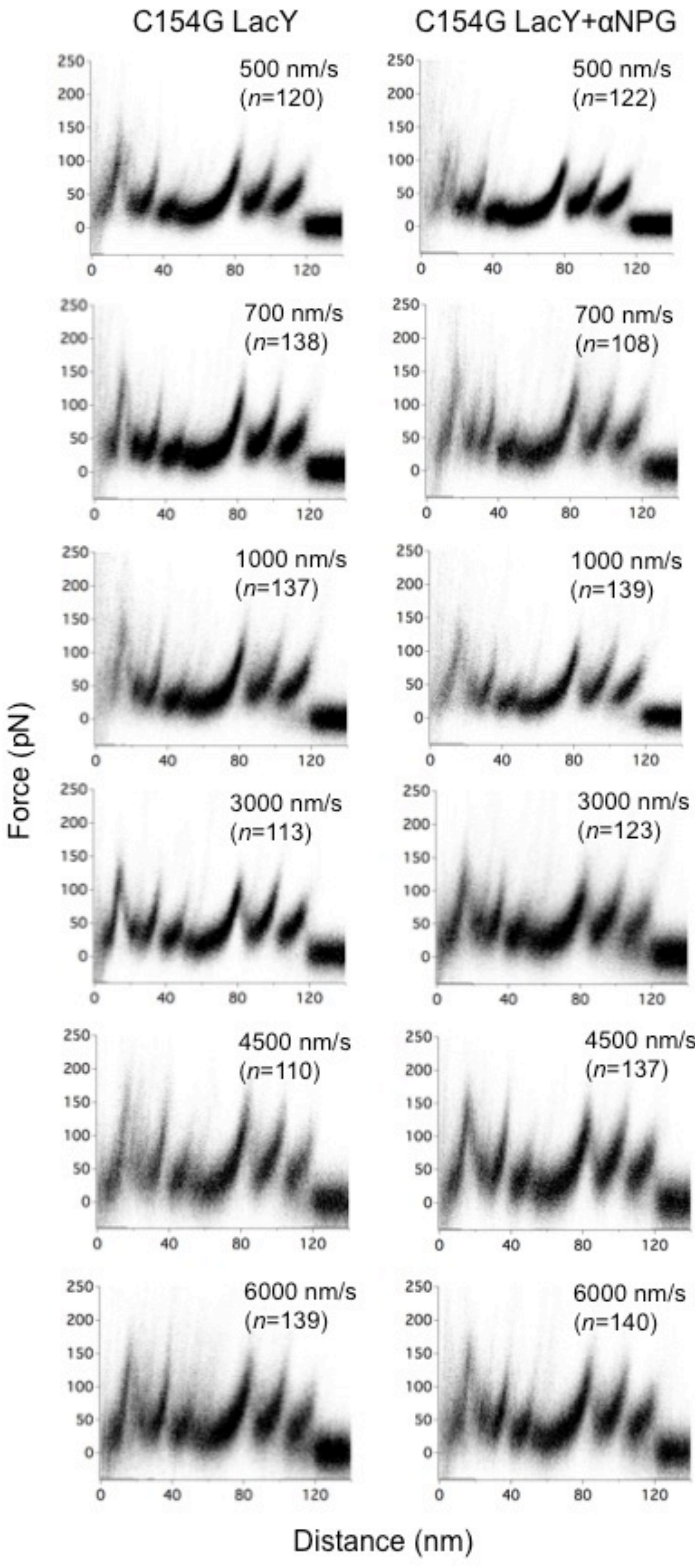

Fig. S7. Superimposed F-D curves recorded on unfolding of mutant C154G LacY reconstituted into POPE:POPG (3:1) liposomes and in the absence and presence of substrate (αNPG). Superimposed F-D curves are displayed as density plots. Pulling velocities and numbers (*n*) of superimposed F-D curves are indicated. F-D curves are aligned at three prominent force peaks detected at contour lengths of 270 aa, 338 aa, and 404 aa. The full gray scale corresponds to 50 counts. Data were recorded in buffer solution (50 mM KP_i, without or with 1 mM αNPG, pH 7.2) and at ≈25°C.

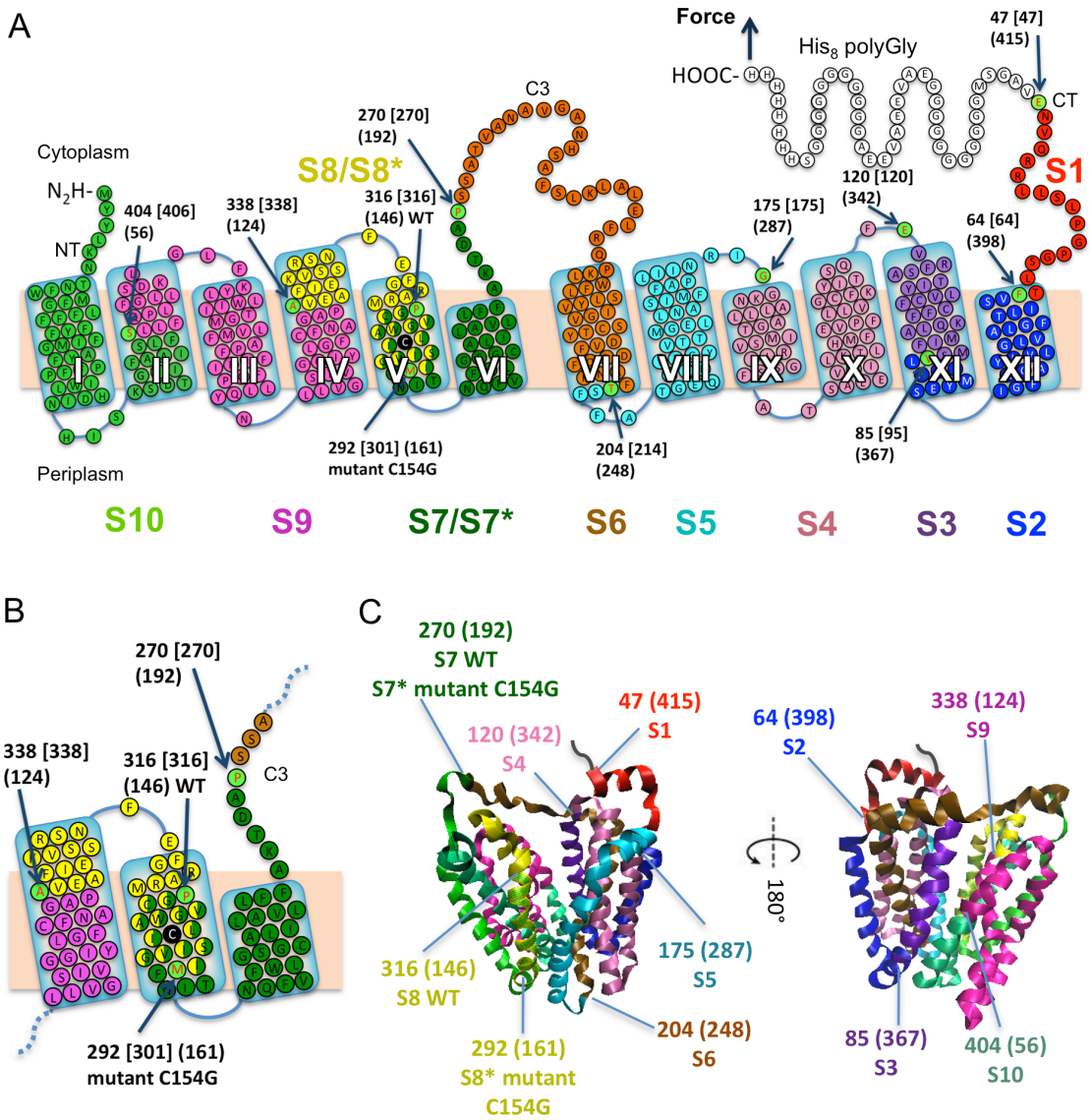

Fig. S8. Stable structural segments mapped to the secondary and tertiary structure model of WT and mutant C154G LacY. (***A***) Secondary structure model mapped with stable structural segments S1-S10. Whereas, stable structural segments S7* and S8* detected for mutant C154G are different from S7 and S8 detected for WT LacY (**Fig. 3**), all other structural segments detected for mutant C154G and WT LacY are the same. Each mean contour length of a force peak class of the force peak histograms (**Fig. 2**) assigns the beginning of a stable structural segment (blue arrows pointing to aa). Black numbers at arrows indicate the mean contour lengths of a force peak class (in aa), numbers in square brackets indicate the aa position counted from the C-terminal end, and numbers in parentheses give the aa position from the N-terminal end. Each of these numbers assigns the end of the previous and the beginning of a new stable structural segment. To obtain their location, the length of polyGly linker and the His-tag is taken into account. If the beginning/end of a stabilizing structural segment locates on the mica-facing side of the membrane or within the membrane the thickness of the membrane is considered (4). All force peaks detected for WT and mutant C145G are the same within experimental error except for the force peak at 316 aa that is detected only in WT LacY and the force peak at 292 aa that is detected only in mutant C145G LacY (**Fig. 2, 6**). Transmembrane helices are labeled I-XII, N-terminus NT, C-terminus CT, and the unstructured C-terminal extension [GSM(G_{11})EAVEEAVEEA(G_{11})S] polyGly with the 8 His-tag His_8 polyGly. (***B***) Close up of the stable structural segments detected at helices IV-VI. Residue C154, which is replaced by a glycine in mutant C154G LacY, is colored black. (***C***) Stable structural segments mapped to the tertiary structure of LacY. The tertiary structure is viewed from two different sides. Each color represents a stable structural segment localized in (***A***). Colored numbers give mean contour lengths of force peak classes, numbers in parentheses give the aa position from the N-terminal end, and abbreviations name the stable structural segment. The

structural segments stabilizing WT and mutant C154G LacY are the same except those detected by the two force peaks at 316 aa and 292 aa. Structural models show LacY from *E. coli* (PDB ID code 1PV7) in the inward-facing conformation (5).

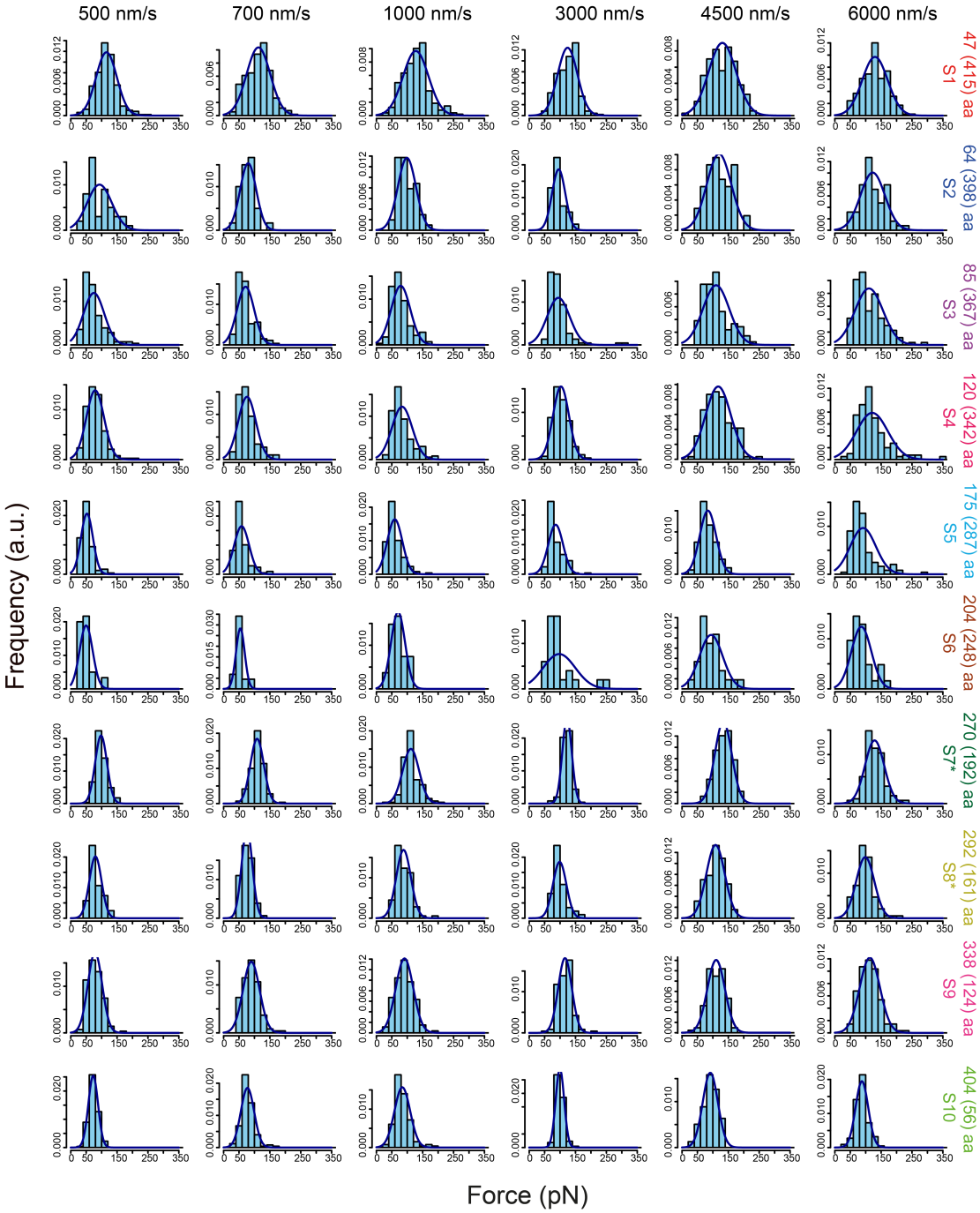

Fig. S9. Forces of unfolding force peaks recorded upon unfolding of mutant C154G LacY in the absence of substrate. Histograms show the force distribution of every unfolding force peak recorded for six different pulling velocities (500, 700, 1000, 3000, 4500, and 6000 nm/s). Colored numbers on the right side give mean contour lengths (in aa) obtained by fitting the force peak classes from contour length histograms (comp. **Fig. 6**), numbers in parentheses give the amino acid position at which a stable structural segment (labeled S1-S10) starts in LacY. The bin size of all histograms is 20 pN. Dark blue lines are Gaussian fits of force distributions. The DFS data is revealed analyzing the FD curves shown in **Fig. S7**.

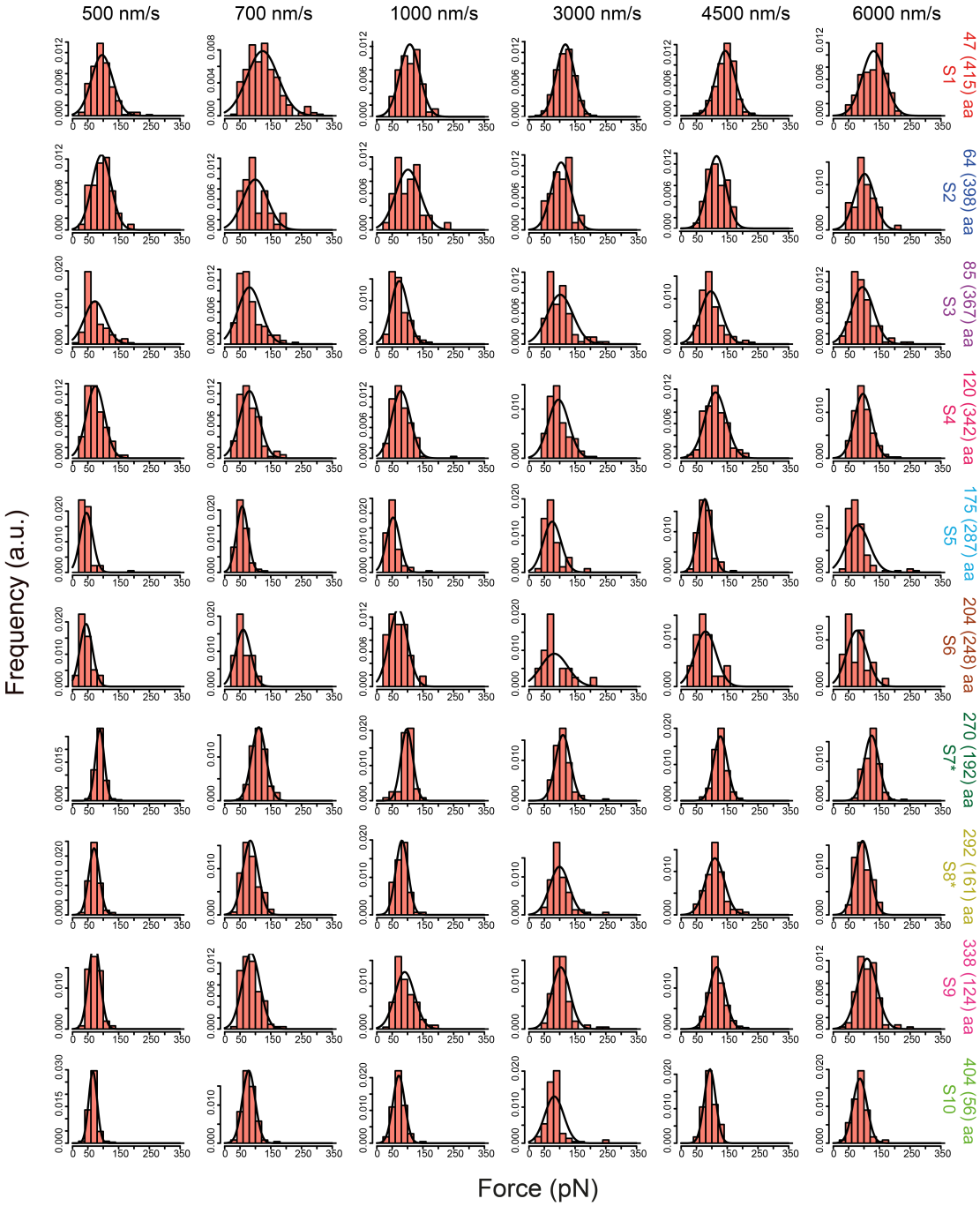

Fig. S10. Forces of unfolding force peaks recorded upon unfolding of mutant C154G LacY in the presence of substrate (αNPG). Histograms show the force distribution of every unfolding force peak recorded for six different pulling velocities (500, 700, 1000, 3000, 4500, and 6000 nm/s). Colored numbers on the right side give mean contour lengths (in aa) obtained by fitting the force peak classes from contour length histograms (comp. **Fig. 6**), numbers in parentheses give the amino acid position at which a stable structural segment starts in LacY. The bin size of all histograms is 20 pN. Dark blue lines are Gaussian fits of force distributions. The DFS data is obtained analyzing the FD curves shown in **Fig. S7**.

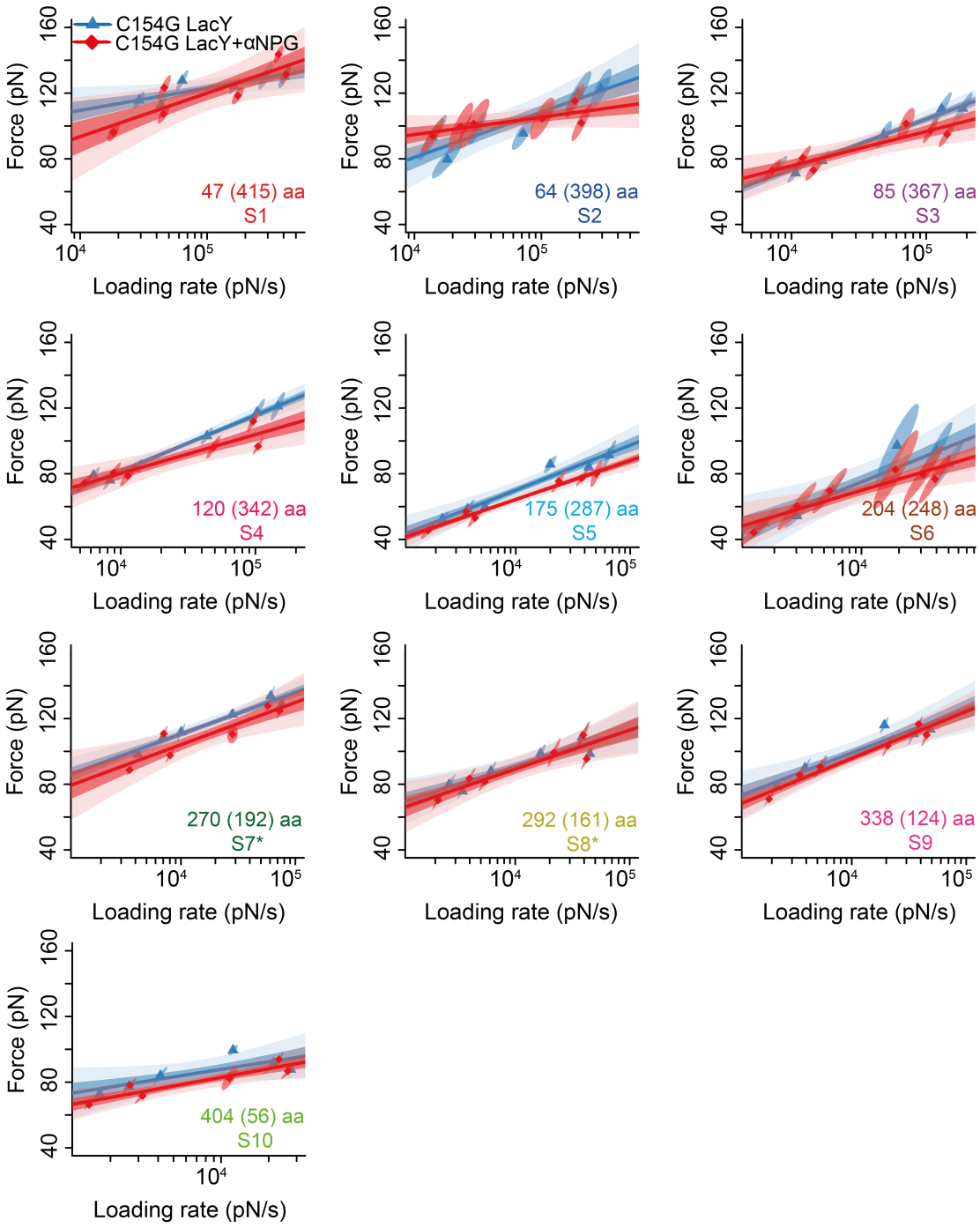

Fig. S11. Substrate binding hardly modulates the interactions stabilizing the structural segments of mutant C154G LacY. Shown are DFS plots of each structural segment (labeled S1-S10) stabilizing C145G mutant LacY reconstituted into liposomes. Colored numbers in each graph give mean contour lengths (in aa) obtained by fitting the force peak classes from contour length histograms (comp. **Fig. 6**), numbers in parentheses give the amino acid position at which a stable structural segment starts in LacY. Each DFS plot describes the dynamic behavior of a stable structural segment in the absence (blue) and in the presence (red) of substrate αNPG. Plotted is the mean unfolding force of each stable structural segment *versus* the mean loading rate. Slanted ellipses indicate one standard error of each data point. The Bell-Evans model is fitted (solid lines) to the DFS plots to obtain the unfolding energy barrier parameters (Methods; **Equations 3 and 4**). Dark- and light-colored regions indicate fitting confidence intervals of one (68%) and two (95%) standard deviations, respectively. The DFS data is obtained analyzing the FD curves shown in **Fig. S7**.

Table S1. Parameters characterizing the free-energy barrier (x_u, k_0, ΔG) and spring constant (κ) of stable structural segments S1-S10 of WT LacY and mutant C154G LacY in the absence and presence of substrate (αNPG). The force peak positions give the mean contour lengths obtained by fitting force peak histograms of WT and mutant C154G LacY in the unbound state (**Fig. 2*C***). Exceptions are the force peaks at 316 aa and 292 aa detected for WT LacY and mutant C154G LacY, respectively. Numbers in parentheses give the amino acid position in the LacY structure at which a stable structural segment starts. Differences between bound and unbound states are considered significant and highlighted by stars when *P*-values approach <0.05 from Analysis of Covariance (ANCOVA) test (see Methods). Errors represent SDs. For each stable structural segment (labeled S1-S10) we also give the secondary structure elements involved (in square brackets). Whereas, stable structural segments S7* and S8* detected for mutant C154G are different from S7 and S8 detected for WT LacY, all other structural segments detected for mutant C154G and WT LacY are the same. Transmembrane helices are named H1-H12, cytoplasmic polypeptide loops C1-C5, periplasmic polypeptide loops P1-P6, N-terminus NT, and C-terminus CT.

Force peak position (aa)	Stable structural segment	x_u (nm)			
		WT	WT+αNPG	C154G	C154G+αNPG
47 (415)	S1 = [CT]	0.31±0.12	0.36±0.10	0.33±0.04	0.35±0.09
64 (398)	S2 = [P6-H12]	0.37±0.09	0.40±0.05	0.37±0.06	0.42±0.03
85 (367)	S3 = [H11]	0.27±0.05	0.56±0.13*	0.31±0.03	0.44±0.04
120 (342)	S4 = [H9-P5-H10-C5]	0.25±0.02	0.48±0.09*	0.28±0.02	0.32±0.01*
175 (287)	S5 = [P4-H8-C4]	0.26±0.01	0.53±0.07*	0.36±0.02	0.39±0.03*
204 (248)	S6 = [C3.2-H7]	0.30±0.10	0.98±0.46*	0.31±0.07	0.36±0.07
270 (192)	S7 = [H5.2-P3-H6-C3.1]	0.28±0.04	0.95±0.12*	-	-
316 (146)	S8 = [H4.2-C2-H5.1]	0.29±0.01	1.24±0.50*	-	-
270 (192)	S7* = [P3-H6-C3.1]	-	-	0.37±0.04	0.37±0.08
292 (161)	S8* = [H4.2-C2-H5]	-	-	0.45±0.03	0.41±0.10
338 (124)	S9 = [H2.2-C1-H3-P2-H4.1]	0.30±0.03	0.81±0.21*	0.36±0.06	0.33±0.04
404 (56)	S10 = [NT-H1-P1-H2.1]	0.41±0.03	0.84±0.12*	0.51±0.04	0.51±0.03

Force peak position (aa)	Stable structural segment	k_0 (s^{-1})			
		WT	WT+αNPG	C154G	C154G+αNPG
47 (415)	S1 = [CT]	0.57±0.33	0.10±0.02	0.35±0.28	0.50±0.14
64 (398)	S2 = [P6-H12]	1.17±0.09	0.10±0.11	0.67±0.91	0.12±0.08
85 (367)	S3 = [H11]	4.36±3.13	0.02±0.07*	2.86±1.41	0.42±0.33
120 (342)	S4 = [H9-P5-H10-C5]	2.84±1.05	0.03±0.00*	2.70±1.02	1.57±0.50*
175 (287)	S5 = [P4-H8-C4]	6.13±0.91	0.13±0.10*	2.14±0.57	1.87±0.76*
204 (248)	S6 = [C3.2-H7]	2.73±4.45	<0.01±0.01*	2.68±2.77	1.71±1.56
270 (192)	S7 = [H5.2-P3-H6-C3.1]	0.71±0.60	<0.01±0.01*	-	-
316 (146)	S8 = [H4.2-C2-H5.1]	1.37±0.28	<0.01±0.01*	-	-
270 (192)	S7* = [P3-H6-C3.1]	-	-	0.04±0.04	0.08±0.16
292 (161)	S8* = [H4.2-C2-H5]	-	-	0.05±0.03	0.09±0.05
338 (124)	S9 = [H2.2-C1-H3-P2-H4.1]	0.50±0.37	<0.01±0.01*	0.17±0.22	0.35±0.28
404 (56)	S10 = [NT-H1-P1-H2.1]	0.12±0.06	<0.01±0.01*	0.02±0.01	0.05±0.02

Force peak position (aa)	Stable structural segment	ΔG ($k_B T$)			
		WT	WT+αNPG	C154G	C154G+αNPG
47 (415)	S1 = [CT]	21.28±0.58	23.02±0.21	21.76±0.78	21.41±0.28
64 (398)	S2 = [P6-H12]	22.47±0.50	23.05±1.15	21.12±1.36	22.84±0.65
85 (367)	S3 = [H11]	19.25±0.72	24.77±4.33*	19.67±0.49	21.60±0.78
120 (342)	S4 = [H9-P5-H10-C5]	19.68±0.37	24.16±0.12*	19.73±0.38	20.27±0.32*
175 (287)	S5 = [P4-H8-C4]	18.91±0.15	22.74±1.11*	19.96±0.27	20.09±0.40*
204 (248)	S6 = [C3.2-H7]	19.72±1.63	28.45±2.62*	19.74±1.03	20.18±0.91
270 (192)	S7 = [H5.2-P3-H6-C3.1]	21.06±0.84	37.5±2.36*	-	-
316 (146)	S8 = [H4.2-C2-H5.1]	20.41±0.20	38.29±6.08*	-	-
270 (192)	S7* = [P3-H6-C3.1]	-	-	23.93±1.06	23.26±1.99
292 (161)	S8* = [H4.2-C2-H5]	-	-	23.70±0.53	22.94±0.41
338 (124)	S9 = [H2.2-C1-H3-P2-H4.1]	21.42±0.74	33.95±0.43*	22.51±1.32	21.76±0.78
404 (56)	S10 = [NT-H1-P1-H2.1]	22.83±0.47	32.53±3.31*	24.69±0.73	23.78±0.51

Force peak position (aa)	Stable structural segment	κ (N/m)			
		WT	WT+αNPG	C154G	C154G+αNPG
47 (415)	S1 = [CT]	1.81±0.70	1.49±0.27	1.62±0.36	1.44±0.37
64 (398)	S2 = [P6-H12]	1.31±0.19	1.20±0.34	1.30±0.12	1.05±0.26
85 (367)	S3 = [H11]	2.13±0.37	0.66±0.25*	1.67±0.14	0.92±0.08
120 (342)	S4 = [H9-P5-H10-C5]	2.57±0.63	0.85±0.43*	2.09±0.14	1.66±0.17*
175 (287)	S5 = [P4-H8-C4]	2.39±0.08	0.67±0.09*	1.26±0.06	1.03±0.04*
204 (248)	S6 = [C3.2-H7]	1.80±0.32	0.24±0.29*	1.70±0.13	1.31±0.10
270 (192)	S7 = [H5.2-P3-H6-C3.1]	2.15±0.12	0.33±0.44*	-	-
316 (146)	S8 = [H4.2-C2-H5.1]	1.99±0.40	0.21±0.13*	-	-
270 (192)	S7* = [P3-H6-C3.1]	-	-	1.41±0.08	1.40±0.07
292 (161)	S8* = [H4.2-C2-H5]	-	-	0.96±0.03	1.01±0.08
338 (124)	S9 = [H2.2-C1-H3-P2-H4.1]	1.92±0.10	0.41±0.15*	1.47±0.16	1.62±0.13
404 (56)	S10 = [NT-H1-P1-H2.1]	1.10±0.07	0.36±0.07*	0.78±0.05	0.76±0.04

APPENDIX 1: SMFS data analysis.

Every unfolding force peak of each FD curve was fitted using the worm-like-chain (WLC) model (6) with a persistence length of 0.4 nm and an aa length of 0.36 nm (7). The WLC fit of each unfolding force peak provides the contour length that reflects the amount of amino acids unfolded and stretched. The contour lengths and rupture forces of all unfolding force peaks were statistically analyzed and displayed in histograms. These histograms showing the probability of force peaks to be detected at particular contour length were normalized. Force peak histograms were fitted applying the Gaussian mixture model (8). In terms of this model, each *i*-th observed contour length l_i stems from one force peak class s = 1,…., M with probability π_s or from background noise with probability π_0. For Lacy force peak histograms were fitted using a mixture of 10 different force peak classes, each at a certain contour length. Therefore, the contour length for a given force peak class s can be described by a Gaussian distribution with mean contour length μ_s and variance σ_s^2. Taking into account that it is unknown to which force peak class a contour length belongs, the probability density f of l_i can be presented as a mixture of Gaussians and background noise with weights π_s and π_0 correspondingly.

$$f(l_i) = \sum_{s=1}^{M} \pi_s \phi(l_i, \mu_s, \sigma_s^2) + \pi_0 g(l_i) \quad \text{(Equation 1)}$$

where $\phi(l_i, \mu_s, \sigma_s^2)$ is the probability density of the Gaussian distribution and $g(l_i)$ the background noise. The expectation optimization algorithm was used to distinguish parameters of the model (π, μ, σ^2). The most probable force peak class s_i was assigned to any given contour length l_i with the Bayes classifier by setting:

$$s_i = argmax_s\ (\pi_s \phi(l_i, \mu_s, \sigma_s^2), \pi_0 g(l_i)) \quad \text{(Equation 2)}$$

All observed contour lengths were assigned to the force peak classes. For each pulling velocity the mean unfolding force and loading rate were determined.

APPENDIX 2: Calculation of energy landscape parameters and mechanical rigidity.

The Bell-Evans model (9, 10) was applied to analyze the DFS data. According to the model, the most probable force F at which a folded structure transits from the native folded to the unfolded state depends on the loading rate r_{sv} (Eq. 3)

$$F_{sv} = \frac{k_B T}{x_u} \ln\left(\frac{x_u r_{sv}}{k_B T\, k_0}\right) \quad \text{(Equation 3)}$$

where k_B is the Boltzmann constant, T the absolute temperature, r_{sv} the most probable loading rate, x_u the distance between native and transition state, k_0 the loading rate at zero force (*e.g.*, equilibrium). Loading rate had been taken as $r_{sv}=k_{spacer}*v$, where v is the pulling velocity. Experimental loading rate and force distribution histograms were fitted by Gaussian distributions (**Fig. S5, S6, S9, S10**). Linear regression of the Bell-Evans equation was applied to the DFS plot of every structural segment (**Fig. S6, S11**). Taking into account the uncertainty in both F_{sv} and r_{sv} the reciprocals of the determinant of the covariance matrices for the pulling velocity are used as weighting coefficients in the DFS plot. x_u and k_0 were calculated from the slope and intercept of the DFS fit.

The height of the free energy barrier was calculated using an Arrhenius equation

$$\Delta G = -k_B T \ln(\tau_D k_0) \quad \text{(Equation 4)}$$

Where τ_D represents the diffusive relaxation time with $\tau_D \approx 10^{-9}$ s taken for this work (11). In the absence of any information on the energy potential shape, we applied a simple parabolic potential. Accordingly, the spring constant of the structural segment stabilized by the barrier κ can be estimated by:

$$\kappa = \frac{2\Delta G}{x_u^2} \quad \text{(Equation 5)}$$

Errors in ΔG were estimated for propagation of errors in k_0, errors in ΔG and x_u were estimated by propagation of errors in κ.

Analysis of covariance (ANCOVA) was performed to test if the difference between linear regressions of different DFS data sets (**Fig. S6, S11**) is significant. First, a *P*-value (two-tailed) testing the null hypothesis that two DFS slopes show no different linear regressions was calculated. If $P < 0.05$ two DFS slopes are considered to be significantly different. If DFS slopes are indistinguishable, they could be parallel with distinct intercepts. Thus, a second *P*-value testing the null hypothesis whether two DFS slopes are identical in sense of intercepts was done. If the DFS slopes and intercepts are not significantly different then single slope and intercept could be calculated for all the linear regressions.

Supporting References

1. Muller DJ & Engel A (2007) Atomic force microscopy and spectroscopy of native membrane proteins. *Nat Protoc* 2:2191-2197.
2. Oesterhelt F*, et al.* (2000) Unfolding pathways of individual bacteriorhodopsins. *Science* 288:143-146.
3. Kedrov A, Janovjak H, Sapra KT, & Muller DJ (2007) Deciphering molecular interactions of native membrane proteins by single-molecule force spectroscopy. *Annu Rev Biophys Biomol Struct* 36:233-260.
4. Muller DJ*, et al.* (2002) Stability of bacteriorhodopsin alpha-helices and loops analyzed by single-molecule force spectroscopy. *Biophys J* 83:3578-3588.
5. Abramson J*, et al.* (2003) Structure and mechanism of the lactose permease of Escherichia coli. *Science* 301:610-615.
6. Bustamante C, Marko JF, Siggia ED, & Smith S (1994) Entropic elasticity of lambda-phage DNA. *Science* 265:1599-1600.
7. Rief M, Gautel M, Oesterhelt F, Fernandez JM, & Gaub HE (1997) Reversible unfolding of individual titin immunoglobulin domains by AFM. *Science* 276:1109-1112.
8. Kawamura S*, et al.* (2013) Kinetic, energetic, and mechanical differences between dark-state rhodopsin and opsin. *Structure* 21:426-437.
9. Evans E & Ritchie K (1997) Dynamic strength of molecular adhesion bonds. *Biophys J* 72:1541-1555.
10. Evans E (2001) Probing the relation between force--lifetime--and chemistry in single molecular bonds. *Annu Rev Biophys Biomol Struct* 30:105-128.
11. Bieri O*, et al.* (1999) The speed limit for protein folding measured by triplet-triplet energy transfer. *Proc Natl Acad Sci U S A* 96:9597-9601.